

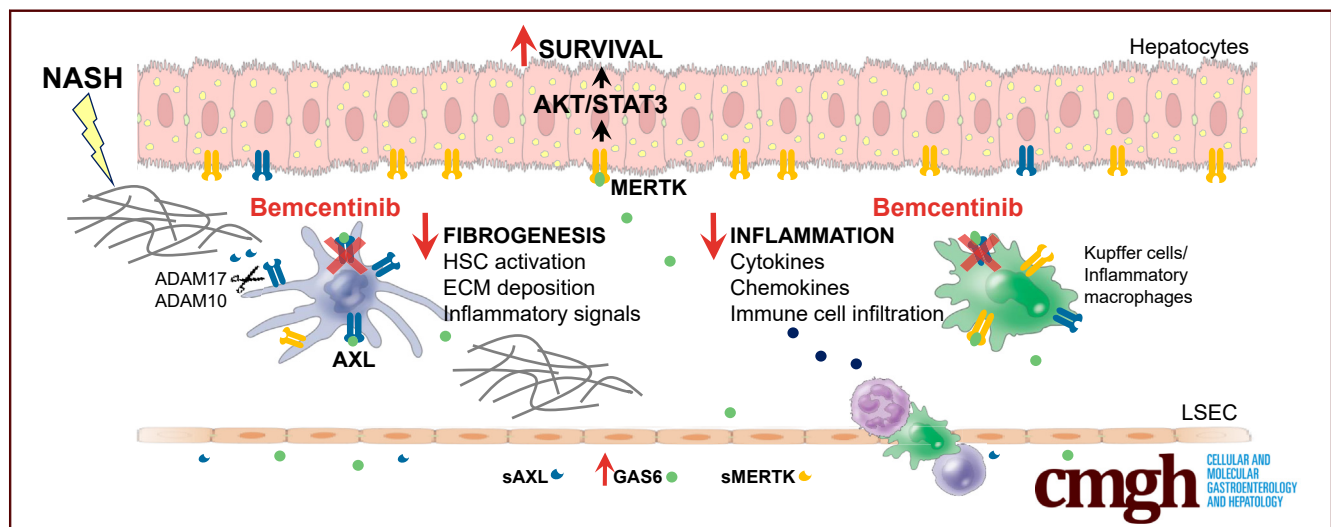
ORIGINAL RESEARCH

A Functional Role of GAS6/TAM in Nonalcoholic Steatohepatitis Progression Implicates AXL as Therapeutic Target



Anna Tutusaus,^{1,2} Estefanía de Gregorio,¹ Blanca Cucarull,^{1,2} Helena Cristóbal,¹ Cristina Aresté,¹ Isabel Graupera,³ Mar Coll,³ Anna Colell,¹ Gro Gausdal,⁴ James B. Lorens,^{4,5} Pablo García de Frutos,¹ Albert Morales,^{1,6} and Montserrat Mari¹

¹Department of Cell Death and Proliferation, Institute of Biomedical Research of Barcelona-Spanish Council of Scientific Research (IIBB-CSIC), August Pi i Sunyer Biomedical Research Institute (IDIBAPS), Barcelona, Spain; ²Departament de Biomedicina, Facultat de Medicina, Universitat de Barcelona, Barcelona, Spain; ³Liver Unit, Hospital Clínic, Biomedical Research Networking Center in Hepatic and Digestive Diseases (CIBERehd), Barcelona, Spain; ⁴BerGenBio AS, Bergen, Norway; ⁵Department of Biomedicine, Centre for Cancer Biomarkers, University of Bergen, Bergen, Norway; and ⁶Barcelona Clinic Liver Cancer Group, Liver Unit, Hospital Clínic, Biomedical Research Networking Center in Hepatic and Digestive Diseases, Barcelona, Spain



SUMMARY

GAS6 signaling through AXL receptor contributes to the progression of nonalcoholic steatohepatitis (NASH). Soluble AXL significantly increases both in NASH patients and mouse models. Experimental AXL inhibition by bemcentinib diminishes inflammation and fibrosis, supporting its therapeutic use in NASH.

BACKGROUND AND AIMS: GAS6 signaling, through the TAM receptor tyrosine kinases AXL and MERTK, participates in chronic liver pathologies. Here, we addressed GAS6/TAM involvement in Non-Alcoholic SteatoHepatitis (NASH) development.

METHODS: GAS6/TAM signaling was analyzed in cultured primary hepatocytes, hepatic stellate cells (HSC) and Kupffer cells (KCs). *Axl*^{-/-}, *Mertk*^{-/-} and wild-type C57BL/6 mice were fed with Chow, High Fat Choline-Deficient Methionine-Restricted (HFD) or methionine-choline-deficient (MCD) diet. HSC activation, liver inflammation and cytokine/chemokine

production were measured by qPCR, mRNA Array analysis, western blotting and ELISA. GAS6, soluble AXL (sAXL) and MERTK (sMERTK) levels were analyzed in control individuals, steatotic and NASH patients.

RESULTS: In primary mouse cultures, GAS6 or MERTK activation protected primary hepatocytes against lipid toxicity via AKT/STAT-3 signaling, while bemcentinib (small molecule AXL inhibitor BGB324) blocked AXL-induced fibrogenesis in primary HSCs and cytokine production in LPS-treated KCs. Accordingly; bemcentinib diminished liver inflammation and fibrosis in MCD- and HFD-fed mice. Upregulation of AXL and ADAM10/ADAM17 metalloproteinases increased sAXL in HFD-fed mice. Transcriptome profiling revealed major reduction in fibrotic- and inflammatory-related genes in HFD-fed mice after bemcentinib administration. HFD-fed *Mertk*^{-/-} mice exhibited enhanced NASH, while *Axl*^{-/-} mice were partially protected. In human serum, sAXL levels augmented even at initial stages, whereas GAS6 and sMERTK increased only in cirrhotic NASH patients. In agreement, sAXL increased in HFD-fed mice before fibrosis establishment, while bemcentinib prevented liver fibrosis/inflammation in early NASH.

CONCLUSION: AXL signaling, increased in NASH patients, promotes fibrosis in HSCs and inflammation in KCs, while GAS6 protects cultured hepatocytes against lipotoxicity via MERTK. Bemcentinib, by blocking AXL signaling and increasing GAS6 levels, reduces experimental NASH, revealing AXL as an effective therapeutic target for clinical practice. (*Cell Mol Gastroenterol Hepatol* 2020;9:349–368; <https://doi.org/10.1016/j.jcmgh.2019.10.010>)

Keywords: Liver Fibrosis; Hepatic Stellate Cells; Bemcentinib (BGB324); GAS6/TAM Signaling; Liver Inflammation.

See editorial on page 545.

Patients with nonalcoholic fatty liver disease (NAFLD), despite being mostly asymptomatic, suffer increased cardiovascular and mortality risk. Among them, individuals with NASH, an increasing liver pathology in developed countries, are predisposed to cirrhosis and liver-related complications.^{1–3} In NASH patients, after cardiovascular disease and liver cancer, cirrhosis is the third leading cause of death and it is expected to be the most common indication for liver transplantation. At present, lifestyle modification with dietary restrictions is the standard of treatment for patients with NASH.⁴ Recently, therapies based on the activation of specific nuclear factors such as LXR (obeticholic acid) or PPAR (elafibranor), or directed against chemokine receptors (cenicriviroc) have obtained positive results in clinical trials.^{5–7} However, there are no approved drug treatments for NAFLD and NASH. Several other emerging therapies aimed to target NASH in a pre-cirrhotic stage, when liver fibrosis and hepatic inflammation are still recoverable, are being tested.⁸ Liver fibrosis, characterized by accumulation of extracellular matrix (ECM) components from activated hepatic stellate cells (HSCs), is associated to chronic liver injury and disease severity.^{9,10} In NASH, fibrosis is accompanied by liver inflammation from both resident macrophages (Kupffer cells [KCs]) and infiltrating cells, remodeling of the microenvironment that promote liver degeneration and tumor development.^{11–13}

Growth arrest-specific gene 6 (GAS6) activates receptor tyrosine kinases AXL, MERTK, and Tyro3, known as TAM receptors, regulates innate immune response and it is implicated in cancer progression.^{14,15} GAS6 shares structural and sequence similarity with the anticoagulant protein S that also binds TAM receptors, however their biological roles differ.¹⁶ In particular, GAS6 has no major role in coagulation and protein S does not activate AXL under physiological conditions. In liver pathologies, GAS6 is hepatoprotective in ischemia/reperfusion-induced damage,¹⁷ and participates in wound healing responses.^{18,19} Hepatic expression of GAS6/AXL is mainly detected in macrophages, including KCs, and in activated HSCs.²⁰ GAS6/AXL participates in HSC activation and in damage by CCl₄ exposure in mice.²¹ In patients, GAS6 and soluble AXL (sAXL) serum levels increase during chronic liver disease progression in alcoholic liver disease, and in hepatitis C virus patients.

Concurrently, messenger RNA (mRNA) expression of MERTK, the other main receptor of GAS6 in the liver, has been associated with liver fibrosis and NASH.^{22,23} This scenario suggests a role of GAS6 signaling in NASH development.²⁴ Our current results reveal that sAXL is increased in all NAFLD stages in human samples, whereas GAS6 and soluble MERTK (sMERTK) are only enhanced in cirrhotic NASH patients. Oral administration of bemcentinib, the first selective small molecule inhibitor of AXL (BGB324) in phase II clinical trials for cancer,²⁵ blocks HSC transdifferentiation and macrophage activation, greatly diminishing liver fibrosis and hepatic inflammation in mice fed with a NASH diet. Our results identify AXL as an interesting serum biomarker of in human NAFLD development and the GAS6/AXL axis as a therapeutically targetable pathway to prevent NASH progression. In summary, our data support specific AXL inhibition as strategy for NASH treatment.


Results

GAS6 Protects Hepatocytes Against Lipotoxicity Via MERTK Activation, While AXL Promotes Liver Fibrosis in HSC and Inflammation in KCs

To study a potential role of GAS6 and their main receptors in the liver AXL and MERTK, we analyzed their signaling in different liver cell populations using recombinant mouse GAS6 and specific activating antibodies²⁶ for AXL and MERTK. First, we tested the specificity of each activator using knockout (KO)- and wild-type (WT)-derived primary fibroblasts, cells that express endogenous levels of both TAM receptors (Figure 1A). α AXL induced AKT phosphorylation only in WT and *Mertk*^{-/-} cells, while α MERTK induced p-AKT only in WT and *Axl*^{-/-} but not in *Mertk*^{-/-} cells, confirming their activation capabilities and specificity.

The hepatoprotective role of GAS6 has been described during hypoxia of primary hepatocytes,¹⁷ so we tested the potential participation of GAS6 signaling in hepatocellular lipotoxicity, which contributes to the liver damage detected in NASH. In primary mouse hepatocytes (PMHs) treated with palmitic acid (PA), GAS6 diminished palmitic-induced PMH cell death, a protection that was similarly

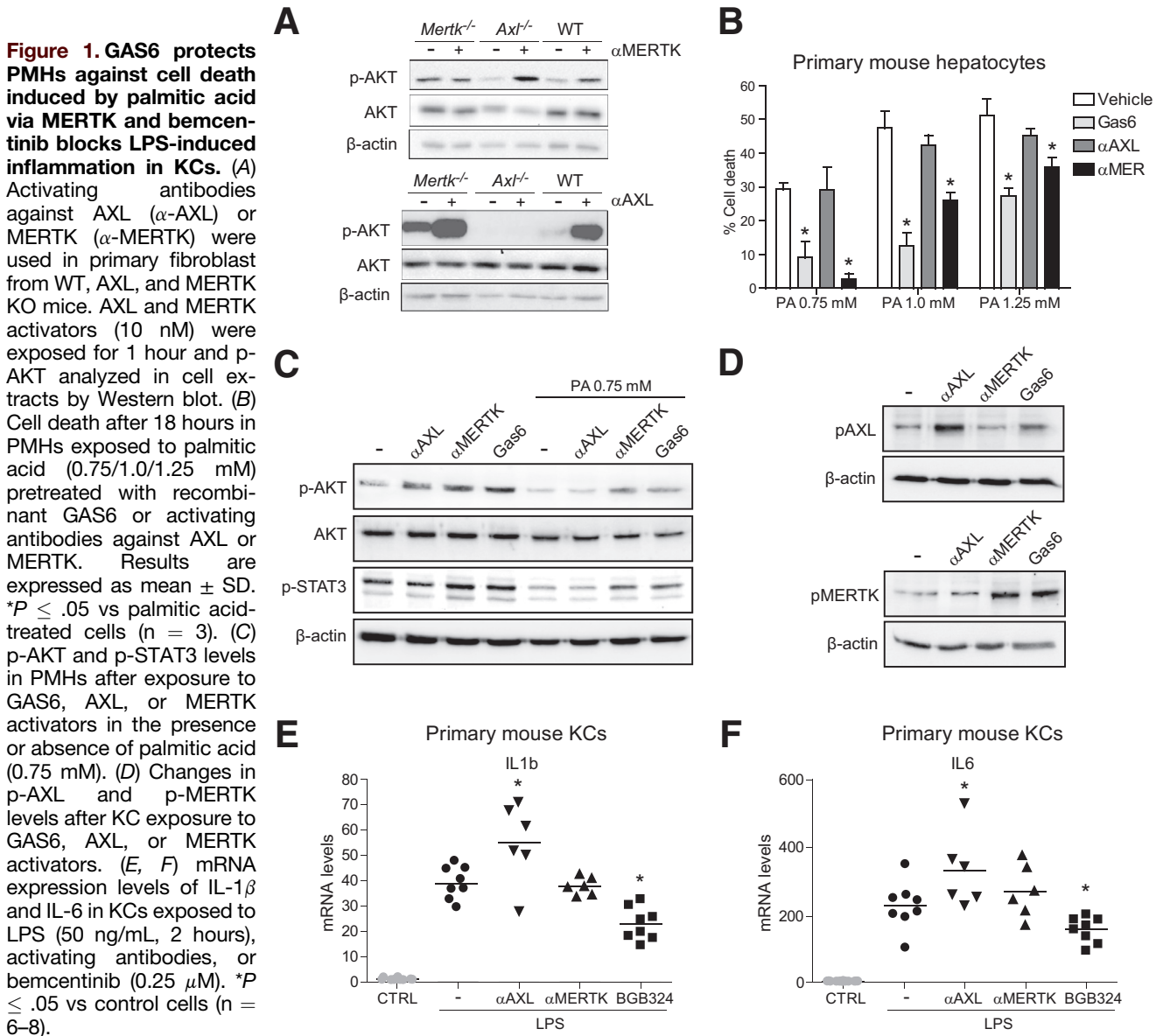
Abbreviations used in this paper: ADAM10, a disintegrin and metalloproteinase 10; ADAM17, a disintegrin and metalloproteinase 17; cDNA, complementary DNA; ECM, extracellular matrix; ELISA, enzyme-linked immunosorbent assay; GAS6, Growth arrest-specific gene 6; H&E, hematoxylin and eosin; HCC, hepatocellular carcinoma; HFD, high-fat choline-deficient methionine-restricted diet; HSC, hepatic stellate cell; IL, interleukin; KC, Kupffer cell; KO, knockout; LPS, lipopolysaccharide; MCD, methionine-choline-deficient diet; MCP-1, monocyte chemoattractant protein-1; MMP9, matrix metalloproteinase-9; MPO, myeloperoxidase; mRNA, messenger RNA; NAFLD, nonalcoholic fatty liver disease; NAS, NAFLD activity score; NASH, nonalcoholic steatohepatitis; PA, palmitic acid; PBS, phosphate-buffered saline; PMH, primary mouse hepatocyte; sAXL, soluble AXL; sMERTK, soluble MERTK; TAM, Tyro3-Axl-Mertk; TNF, tumor necrosis factor; WT, wild-type.

 Most current article

© 2020 The Authors. Published by Elsevier Inc. on behalf of the AGA Institute. This is an open access article under the CC BY-NC-ND license (<http://creativecommons.org/licenses/by-nc-nd/4.0/>).

2352-345X

<https://doi.org/10.1016/j.jcmgh.2019.10.010>



accomplished via MERTK activation (Figure 1B). In contrast, AXL activation did not alter the PA-induced lipotoxicity in PMHs. As previously reported, PA toxicity in PMHs was mediated by AKT and STAT3 de-phosphorylation.²⁷ Interestingly, GAS6 or MERTK not only induced AKT and STAT3 activation, but also were able to rescue p-AKT and p-STAT3 downregulation observed after palmitic acid exposure (Figure 1C). These results point to GAS6 via the MERTK/AKT/STAT3 axis as a mechanism of hepatoprotection against lipotoxicity with potential relevance in NASH.

AXL deficiency has been reported to increase hepatic inflammation after lipopolysaccharide (LPS) or acute carbon tetrachloride (CCl₄) administration,²⁸ in contrast to previous data in chronic liver damage.²¹ To verify this point, we analyzed the effect of AXL or MERTK activation in primary KCs after LPS challenge. First, we verified that GAS6 induced AXL and MERTK activation in primary mouse KCs, while α AXL and α MERTK only induced AXL and MERTK

phosphorylation, respectively (Figure 1D). Of note, LPS upregulation of interleukin (IL)-1 β and IL-6 mRNA in KCs was potentiated exclusively by AXL (Figure 1E, F) but not by MERTK activation. In addition, AXL inhibition reduced IL-1 β and IL-6 gene transcription after LPS exposure. Therefore, AXL plays a proinflammatory action in LPS-primed KCs that could be blocked by bemcentinib administration.

Different studies have shown that GAS6 has a profibrogenic action in HSC. To better differentiate the specific roles of AXL and MERTK, mouse HSCs were exposed to mouse activating antibodies for these receptors and fibrosis-related genes were analyzed. Increased α -SMA and COL1A1 mRNA levels were detected after AXL activation (Figure 2A), a feature that was not observed via MERTK. To validate these results in activated human HSCs, LX2 cells were tested. While recombinant human GAS6 upregulated α -SMA and COL1A1 gene expression in LX2 cells (Figure 2B), GAS6 profibrogenic gene induction was completely abolished by

AXL inhibition with bemcentinib. These results were in agreement with previous observations showing that GAS6 upregulation of fibrosis-related genes through AXL/AKT activation could be abolished by AXL silencing or

pharmacological AXL inhibition.²¹ Bemcentinib completely blocked not only GAS6-dependent α -SMA and COL1A1 expression in LX2 cells, but also monocyte chemoattractant protein-1 (MCP-1) release to the medium (Figure 2C).

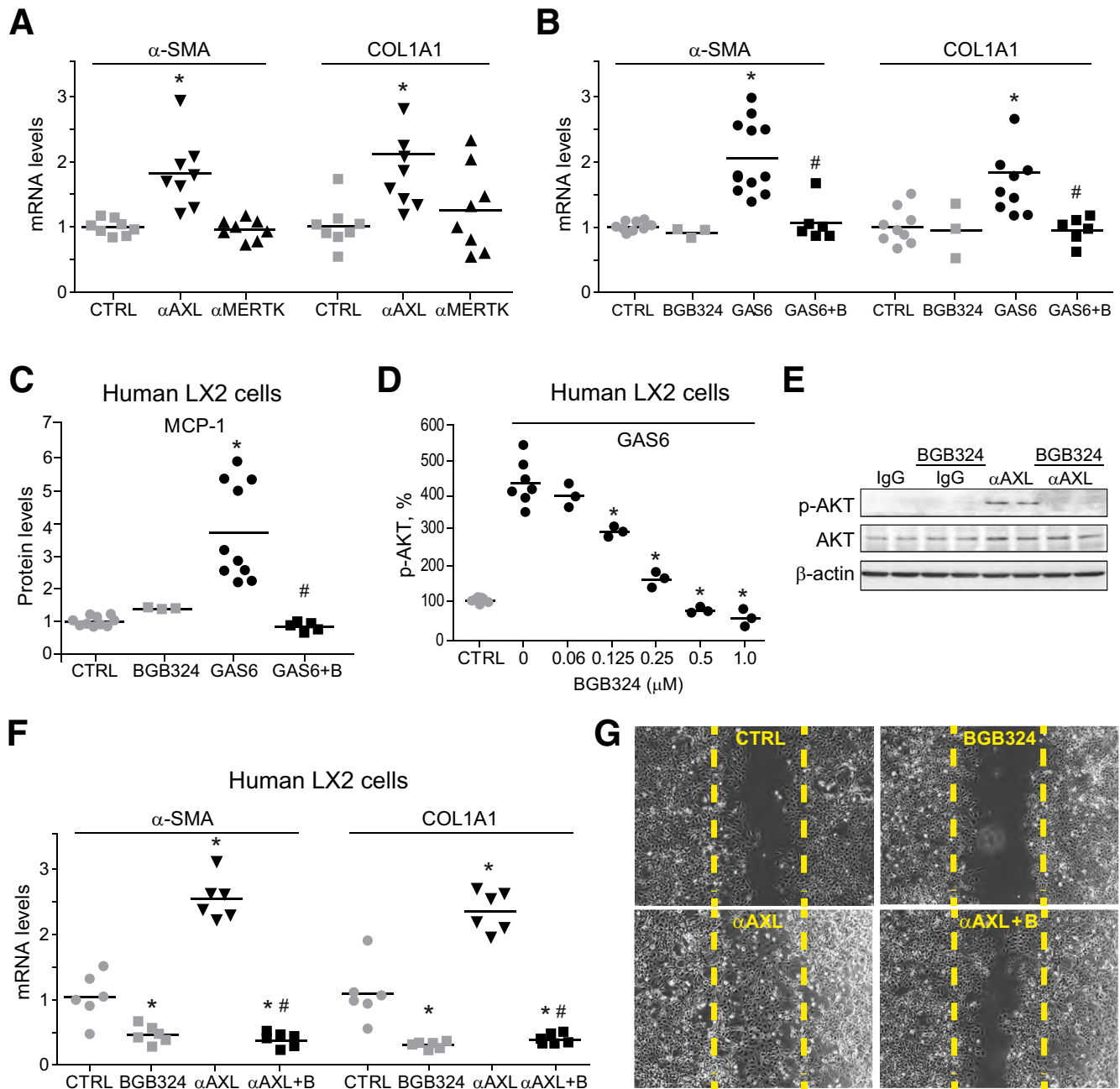


Figure 2. GAS6 and AXL activation induce profibrotic signaling in HSCs, being blocked by bemcentinib administration. α -SMA and COL1A1 mRNA levels in primary HSCs incubated (A) with activating antibodies against AXL or MERTK (10 nM) for 24 hours (n = 8) and (B) after GAS6 and/or bemcentinib incubation (n = 3–12). (C) MCP-1 release measured by ELISA in cultured medium after 16 hours in GAS6-treated (1 μ g/mL) LX2 cells preincubated with BGB324 (0.25 μ M) or vehicle (n = 3–10). (D) p-AKT levels measured by ELISA in LX2 cell extracts after GAS6 addition (1 μ g/mL, 15 minutes) and BGB324 preincubation (0–1.0 μ M) or vehicle (n = 3–8). (E) Representative Western blot of p-AKT and AKT in LX2 cells treated with AXL activating antibody (α -AXL, 10 nM, 15 minutes) and bemcentinib (0.25 μ M). (F) mRNA expression level of α -SMA and COL1A1 in LX2 cells treated with AXL activating antibody (α -AXL, 10 nM, 24 hours) and bemcentinib (0.25 μ M). * $P \leq .05$ vs control cells, # $P \leq .05$ vs α -AXL- or GAS6-treated cells (n = 6). (G) Representative images of cell migration experiments in LX2 cells treated with α -AXL (10 nM, 24 hours) or bemcentinib (0.25 μ M). The percentage of migrated cells was quantified using ImageJ software, establishing as 100% the rate of scratch replenishment after 24 hours in untreated LX2 cells. * $P \leq .05$ vs control cells; # $P \leq .05$ vs GAS6- or α -AXL-treated cells.

Remarkably, this effect was achieved at nanomolar concentration of bemcentinib, which does not affect MERTK phosphorylation,²⁹ being sufficient to eliminate GAS6-dependent AKT activation in LX2 cells (Figure 2D).

To verify that AXL activation is sufficient to induce fibrosis in HSCs, a human activating antibody³⁰ was used in LX2 cells. α AXL induction of AKT phosphorylation (Figure 2E) and the increase expression of α -SMA and COL1A1 (Figure 2F) levels were suppressed by bemcentinib. In contrast, gene expression induced by transforming growth factor β was not blocked by AXL inhibition (data not shown) in agreement with a specific effect on AXL-dependent signaling. Moreover, AXL activation potentiated HSC migration ($325 \pm 36\%$) in scratch assays in LX2 cells, while bemcentinib reduced the motility of activated HSCs ($92 \pm 13\%$), particularly after treatment with α AXL ($169 \pm 10\%$) (Figure 2G). These results reveal the profibrogenic role of AXL in HSC signaling, promoting extracellular matrix modification, macrophage recruitment, and HSC migration. Therefore, the blockage of these pathological AXL-dependent mechanisms by bemcentinib could be an interesting strategy for NASH treatment.

Liver Fibrosis and Inflammation Induced by Methionine- and Choline-Deficient Diet Is Reduced by AXL Inhibition

We analyzed the role of AXL in an experimental murine NASH model. Mice were fed with methionine- and choline-deficient diet (MCD)³¹ during 6 weeks and daily gavaged with vehicle or bemcentinib (BGB324) for the last 2 weeks before sacrifice. Hematoxylin and eosin (H&E) staining of liver samples showed macrovesicular fat in MCD-fed mice and collagen accumulation as visualized with Sirius Red dye (Figure 3A). Fibrosis quantification showed that bemcentinib-treated mice displayed reduced fiber formation after MCD feeding. Similarly, collagen deposition was reduced by bemcentinib administration as measured by hydroxyproline levels (Figure 3B). Transaminase levels (alanine aminotransferase) were similarly increased in all MCD-treated mice (MCD: 204 ± 56 U/L; MCD+BGB324: 212 ± 68 U/L) compared with the control mice (42 ± 6 U/L). In line with fibrosis reduction, α -SMA mRNA levels were decreased in MCD-fed mice receiving bemcentinib (Figure 3C). In addition, diminished expression of inflammatory genes, such as tumor necrosis factor (TNF) or MCP-1, was detected after AXL inhibition in MCD-fed mice, while changes in macrophage population or neutrophil infiltration were not significant (Figure 3C). Despite the positive results observed after AXL inhibition, the progressive animal weakening and body weight loss associated to MCD feeding, without increase in the liver-to-body weight ratio (Figure 3D, E), led us to look for a less harmful diet with better correlation with human NASH.

HFD-Induced Liver Inflammation and Fibrosis Is Decreased by AXL Inhibition

To verify bemcentinib efficacy, we tested a second diet that allowed mice feeding for longer periods of time

(Figure 3A),^{32,33} producing robust liver fibrosis in animals with apparent good condition. Mice under a high-fat (60%) choline-deficient methionine-restricted (0.1%) diet (HFD) increased the liver-to-body weight ratio (Figure 4A), exhibiting extensive liver fibrosis and fatty liver after 2 months. High triglyceride levels (Figure 4B) and liver damage (Figure 4C) were also observed. Bemcentinib administration significantly reduced fibrosis development in the liver as denoted after quantification of Sirius Red staining (Figure 4D) and collagen deposition by hydroxyproline measurement (Figure 4E). Besides the improvement in the fibrosis exhibited by HFD-fed mice treated with bemcentinib, a reduction in the NAFLD activity score (NAS) from marked to moderate activity was evident in bemcentinib-treated animals (Figure 4F). While the steatosis grade and hepatocyte ballooning were not altered, a clear change in lobular inflammation, as denoted by the reduced presence of inflammatory foci, was observed (Figure 4G–I).

In agreement, mRNA levels of different profibrotic genes such as α -SMA, COL1A1, or matrix metalloproteinase-9 (MMP9) were remarkably decreased by AXL inhibition (Figure 5A). α -SMA immunostaining reflected reduced α -SMA protein expression in bemcentinib-treated mice (Figure 5B). Not only was ECM status preserved in bemcentinib-treated mice, but also a clear reduction in proinflammatory genes was detected. After HFD feeding, mRNA levels of the chemokine MCP-1 and its receptor CCR2 and of TNF were lowered by bemcentinib (Figure 5A), as well as neutrophil (myeloperoxidase [MPO]) and macrophage infiltration, as also denoted by F4/80 immunostaining (Figure 5C).

Regarding GAS6/TAM receptors signaling, GAS6, sAXL, and sMERTK serum levels were all increased by the HFD (Figure 6A–C). Of note, bemcentinib administration increased GAS6 serum levels without major changes in sAXL or sMERTK levels.

To further characterize NASH-related genes and identify AXL-dependent mechanisms, we analyzed an mRNA array predesigned for fibrosis- and inflammation-related genes. As observed (Figure 6D), AXL inhibition repressed the expression of numerous NASH-induced mRNAs. Among the genes more markedly affected by bemcentinib, we found not only metalloproteinases, integrins, or collagens, but also cytokines, chemokines, and enzymes that have been related to NASH induction such as lysyl oxidase or urokinase, which participates in extracellular matrix remodeling.

As several metalloproteinases that modify the hepatic ECM are increased in NASH development, we analyzed the mRNA levels of AXL and the a disintegrin and metalloproteinase-10 (ADAM10) and ADAM17,^{34,35} potentially responsible for sAXL serum increases. These shed-dases detach ectodomains of numerous transmembrane growth factors, cytokines, adhesion molecules or metalloproteinases. Among other targets, ADAM10 is needed for Notch signaling, while ADAM17 controls TNF release. In liver samples from NASH mice, AXL transcription was upregulated after HFD-feeding. ADAM10 mRNA expression was also increased, while ADAM17 was apparently

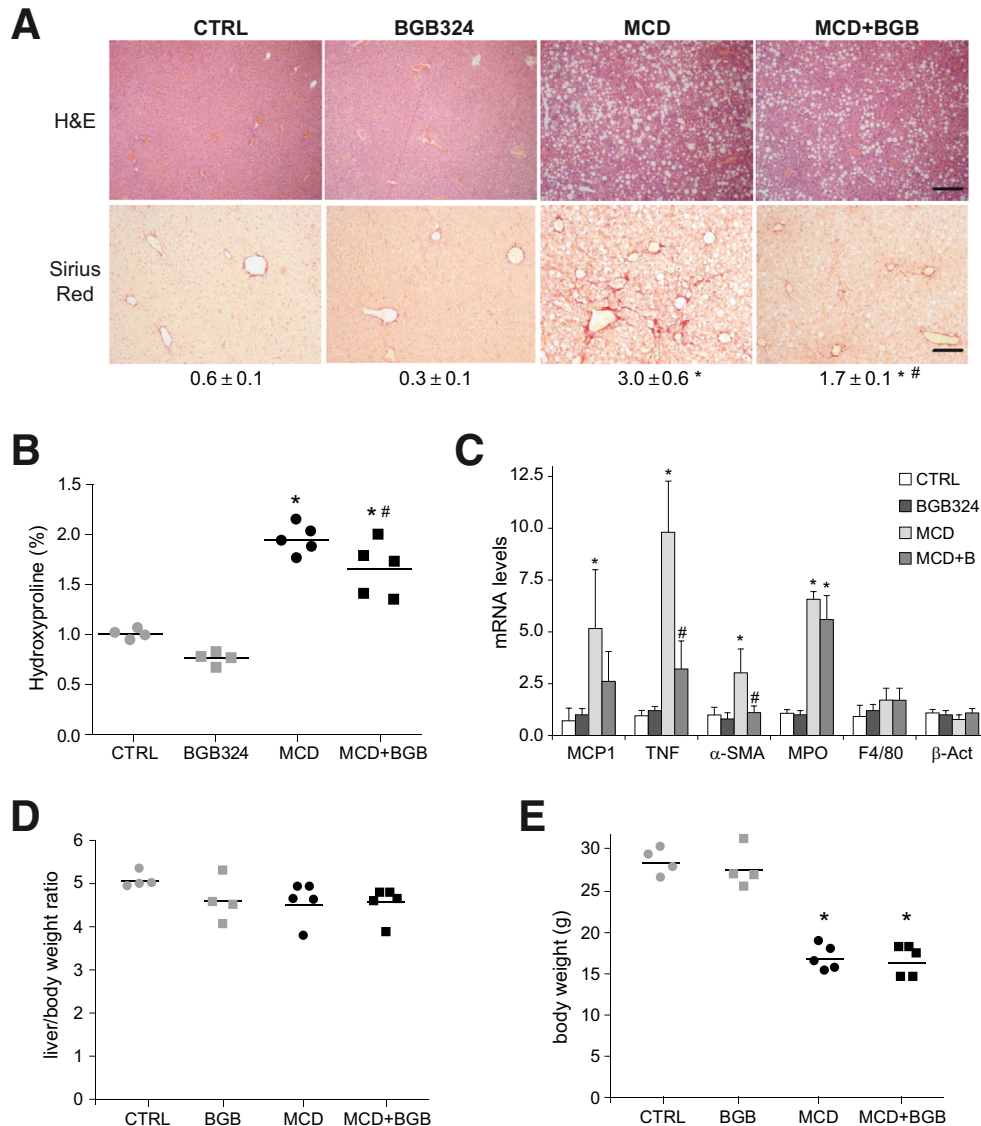
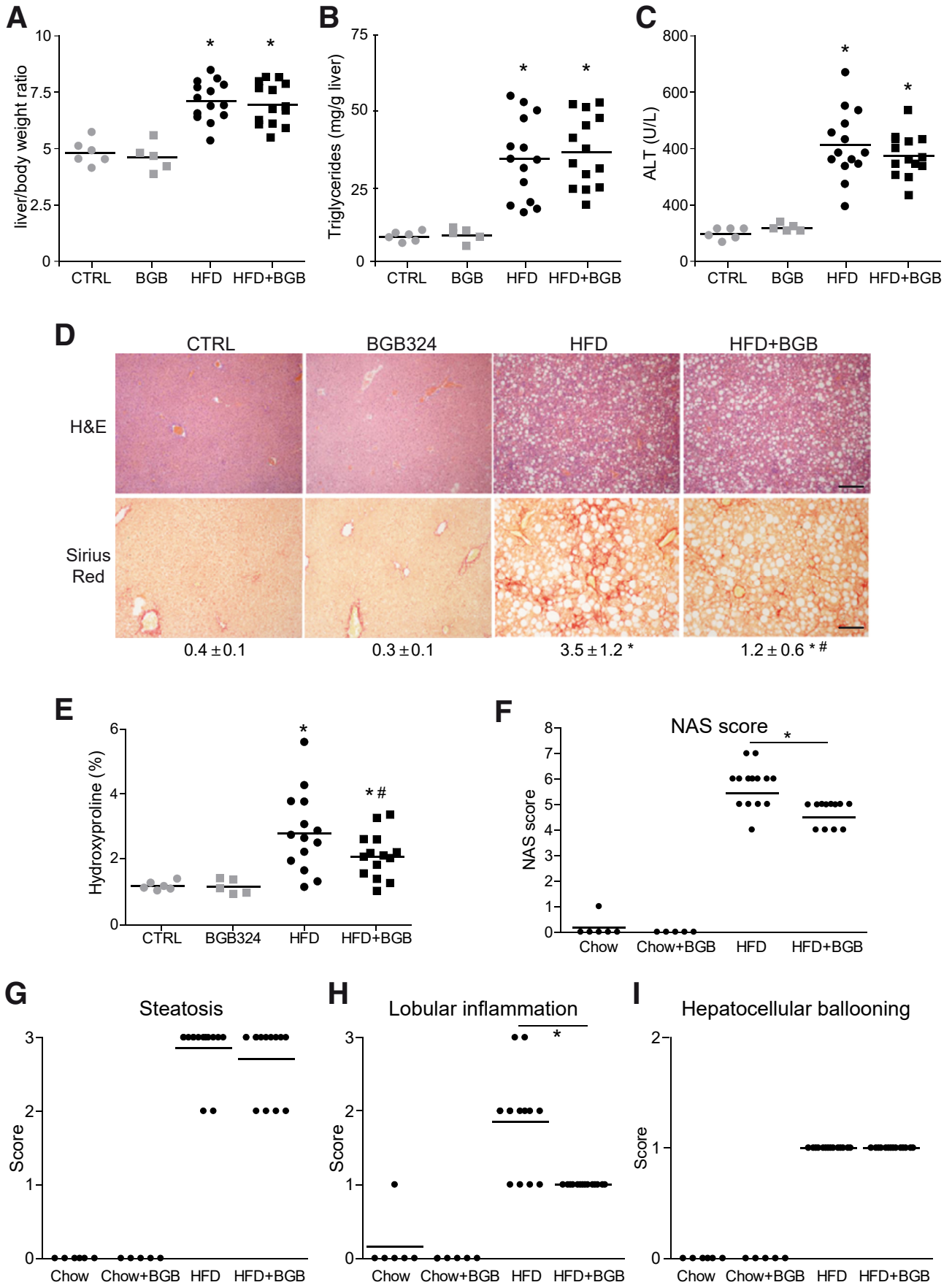


Figure 3. AXL inhibition reduces liver fibrosis and inflammation in MCD-fed mice. (A) Representative images of liver sections after H&E and Sirius Red staining; bar (200 μ m). Sirius Red quantifications using ImageJ software in 6 random sections from each animal are shown below the respective pictures. Student's *t* test; **P* \leq .05 vs control mice, #*P* \leq .05 vs MCD-fed mice; *n* = 5–6 independent samples. (B) Collagen determination by hydroxyproline quantification in liver samples (*n* = 4–5) and (C) mRNA expression level of MCP-1, TNF, α -SMA, MPO, F4/80, and β -actin in liver samples from treated mice. Results are expressed as mean plus standard deviation (*n* = 4–5). **P* \leq .05 vs control mice; #*P* \leq .05 vs MCD-fed mice; Student's *t* test. (D, E) Body and liver weight were measured after sacrifice in mice fed for 6 weeks with chow and MCD diet that received vehicle or bemcentinib (BGB324) oral gavages for the last 2 weeks. **P* \leq .05 vs control; *n* = 4–5. The results shown are representative for 2 independent experiments.

unaffected (Figure 6E). Interestingly, while levels of the precursor (pre) and processed (pro) ADAM10 protein were slightly increased, in accordance to the observed mRNA upregulation, no increment in the active form of ADAM10 was detected by Western blot (Figure 6F). In contrast, ADAM17 protein levels were increased in HFD-fed animals respect to mice fed with chow diet (1.0 ± 0.3 in chow vs 2.3 ± 0.5 in HFD). In line with this protein expression and with previous observations,³⁶ ADAM17 activity was found clearly and significantly increased in liver extracts after HFD feeding (1.1 ± 0.4 vs 2.3 ± 0.2 RFU/ μ g/hour). Moreover, to prove ADAM10/ADAM17 participation in sAXL release, LX2

cells were exposed to ADAM10 or ADAM17 inhibitors and sAXL measured in the medium. AXL release to the medium was almost abrogated by the combination of both inhibitors; being ADAM17 the main contributor to sAXL release in LX2 cells (Figure 6G). These data suggest important roles for these sheddases in TAM signaling during human NASH, particularly for ADAM17, meriting further investigation.

Therefore, the strong induction of liver fibrosis and inflammation observed in mice receiving HFD during 2 months was clearly diminished by bemcentinib administration for the last 2 weeks. Interestingly, HFD increased GAS6, sAXL and sMERTK serum levels, suggesting an



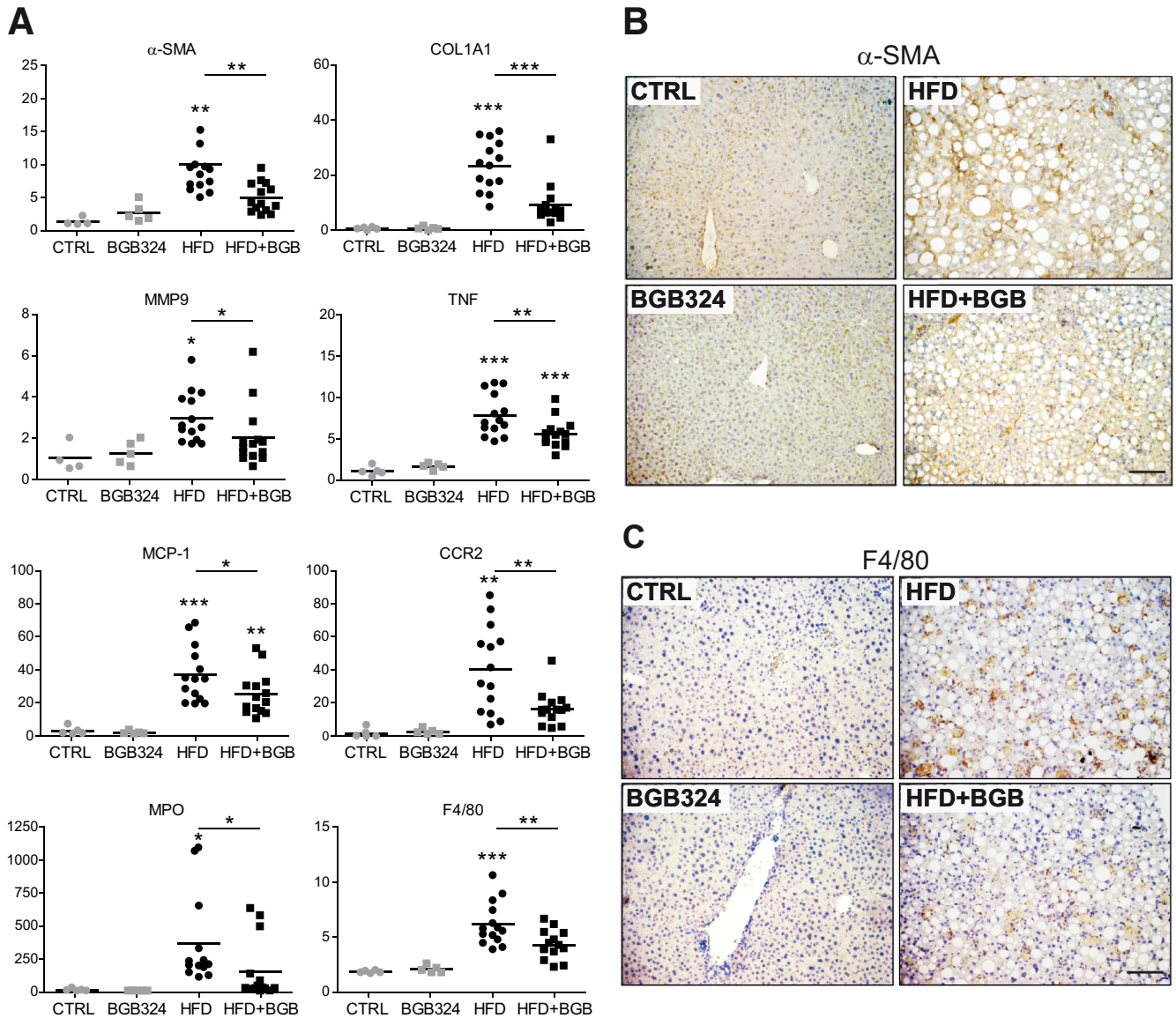


Figure 5. Reduction of profibrotic and proinflammatory gene and protein expression by bemcentinib administration to HFD-fed mice. (A) mRNA expression level of α -SMA, COL1A1, MMP9, TNF, MCP1, CCR2, MPO, and F4/80 were measured in liver samples from animals receiving chow or HFD diet with or without administration of AXL inhibitor bemcentinib. * $P \leq .05$, ** $P \leq .01$, and *** $P \leq .001$ between groups; 1-way analysis of variance; $n = 5-14$. (B, C) Representative images of liver immunohistochemistry of α -SMA and F4/80 expression in mice treated as above. Scale bar = 100 μ m.

upregulation of AXL and MERTK signaling during NASH. Of note, bemcentinib administration not only blocked AXL signaling but also increased GAS6 levels in serum, which could provide hepatocellular protection in addition to AXL inhibition.

AXL Knockout Mice Were Partially Protected Against HFD-Induced Damage While MERTK-Deficient Animals Suffered Aggravated Lesions

Bemcentinib reduced HFD-induced liver fibrosis and inflammation by blocking AXL signaling while increasing

Figure 4. (See previous page). Bemcentinib reduces liver fibrosis and inflammation in HFD-fed mice. (A) Body and liver weight, (B) triglycerides in liver extracts, and (C) serum alanine aminotransferase (ALT) transaminases were measured after sacrifice in mice fed for 8 weeks with chow or HFD that received vehicle or bemcentinib (BGB324) oral gavages for the last 2 weeks ($n = 5-14$). (D) Representative images of liver sections after H&E and Sirius Red staining; bar (200 μ m). Sirius Red quantifications are shown each picture. Student's t test; * $P \leq .05$ vs control mice, # $P \leq .05$ vs HFD-fed mice. (E) Hydroxyproline quantification in liver samples from treated mice. Student's t test; * $P \leq .05$ vs control mice, # $P \leq .05$ vs HFD-fed mice; $n = 5-14$. (F) NAFLD activation score, composed by (G) steatosis, (H) lobular inflammation, and (I) hepatocellular ballooning, was evaluated in liver samples from treated mice. One-way analysis of variance; Student's t test; * $P \leq .05$ vs HFD-fed mice; $n = 5-14$.

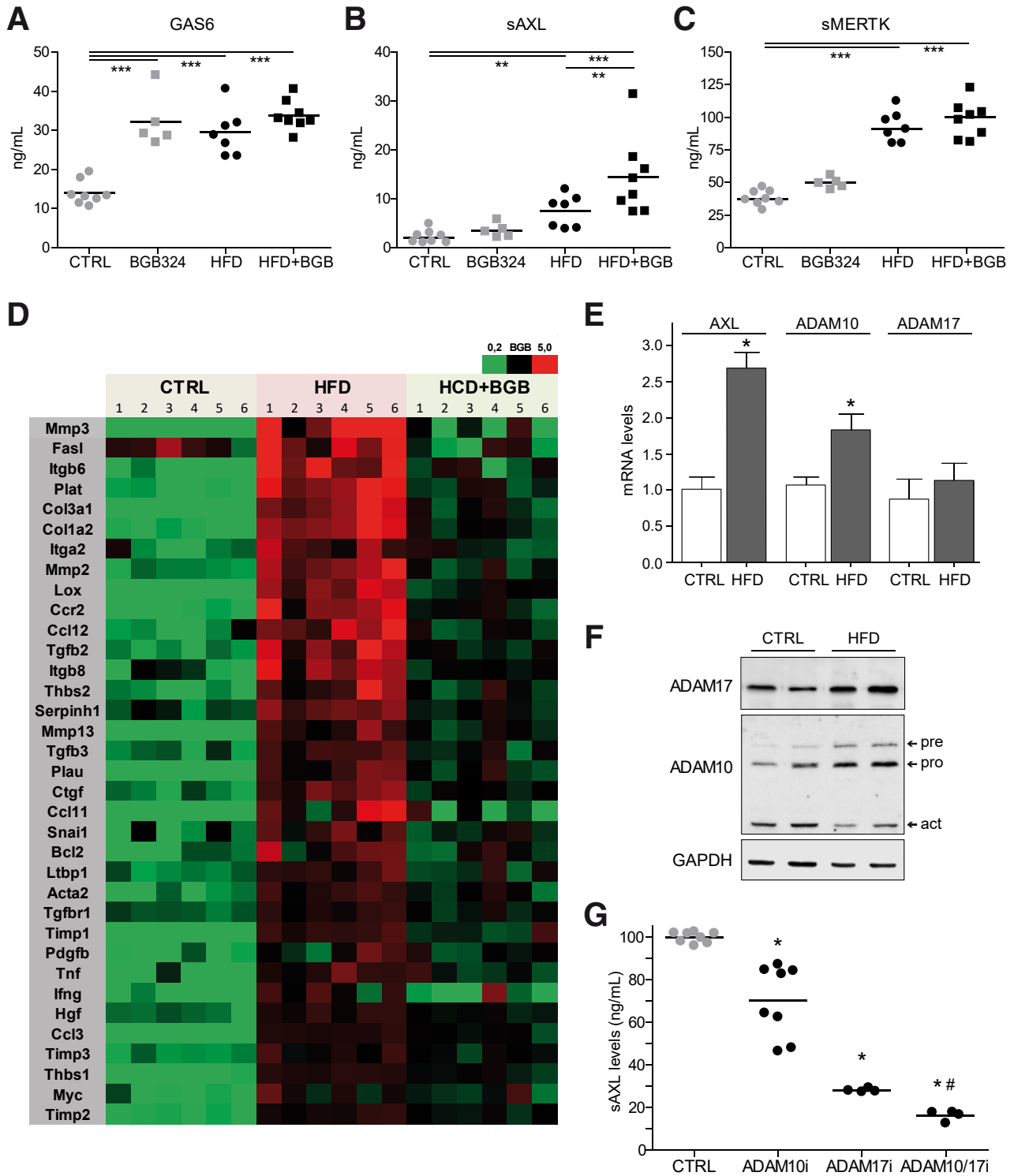


Figure 6. Increased serum sAXL in diet-induced NASH mice as consequence of ADAMs and AXL upregulation. (A–C) Serum GAS6, sAXL, and MERTK levels were measured in mice fed with chow diet and HFD gavaged with vehicle or bemcentinib. * $P \leq .05$, ** $P \leq .01$, and *** $P \leq .001$ between groups; 1-way analysis of variance; $n = 5-8$. (D) Analysis of AXL inhibition in HFD-fed mice using an mRNA Array containing fibrosis- and inflammation-related genes ($n = 6$). (E) Expression changes of AXL, ADAM10, and ADAM17 mRNA in HFD-fed mice. Results are expressed as mean plus standard deviation. * $P \leq .05$ vs control mice; $n = 3$. (F) Representative Western blot of ADAM10, ADAM17, and GAPDH protein expression in chow- and HFD-fed mice. (G) Levels of sAXL secreted from LX2 cells in the presence or absence of ADAM10 inhibitor (GI254023X), ADAM17 inhibitor (TMI-005), or both. * $P \leq .05$ vs untreated cells; # $P \leq .05$ vs ADAM10 or ADAM17 inhibitors; $n = 4-8$.

GAS6 serum levels. To verify if total absence of AXL may recapitulate the protection observed after AXL inhibition, *Axl*^{-/-} mice were fed with HFD for 2 months. After NASH-diet feeding, no significant differences in H&E (Figure 7A) or alanine aminotransferase levels (Figure 7B) were detected between *Axl*^{+/+} and AXL-deficient mice. Although a minor reduction in COL1A1 expression (Figure 7C) and Sirius Red staining (Figure 7A) could be observed in *Axl*^{-/-} mice, did not reach the significance exhibited in bemcentinib-treated mice. In contrast, a decrease in inflammation-related genes (Figure 7D, E) such as TNF or CCR2 was observed in HFD-fed AXL KO mice. In agreement, the NAFLD activation score (Figure 7F) was reduced in HFD-fed *Axl*^{-/-} mice, mostly due to the greater presence of inflammation foci in HFD-fed *Axl*^{+/+} mice (Figure 7G-I). Therefore, the protection detected in AXL-deficient mice did not reach the level observed after bemcentinib treatment, principally due to a minor reduction of the liver fibrosis.

MERTK, the other TAM receptor activated by GAS6 with prominent expression in the liver, has recognized roles in fibrogenesis, inflammation, and hepatoprotection.^{22,23} Evident liver deterioration was detected on H&E slides and in transaminase levels in *Mertk*^{-/-} mice after HFD feeding (Figure 8A, B). In parallel, liver samples from HFD-fed MERTK-deficient mice displayed a significant elevation in collagen deposition compared with HFD-fed WT mice (Figure 8A). Moreover, proinflammatory gene expression was enhanced as denoted by TNF and MPO mRNA levels (Figure 8C, D). In line with these results, NAS was increased in *Mertk*^{-/-} mice (Figure 8E), principally due to higher number of inflammatory foci (Figure 8F-H), underscoring the protective role of MERTK signaling during NASH development and instructing against compounds that could inhibit MERTK in a context of active fibrogenesis and liver inflammation.

AXL Levels Are Increased in the Serum and Liver of NAFLD Patients

GAS6, sAXL, and sMERTK levels have been found altered in patients suffering chronic liver disease.^{21,22,37,38} However, not all 3 measurements have been performed simultaneously in serum from NAFLD patients with different degrees of the disease. Addressing this issue, we detected by enzyme-linked immunosorbent assay (ELISA) increased levels of GAS6, sAXL, and sMERTK in cirrhotic NASH patients (Figure 9A-C), compared with control individuals or patients with low-grade NAFLD (simple steatosis or fibrosis). However, only sAXL was augmented in early stages of NAFLD, when liver fibrosis was still absent, with mean values growing with the severity of the disease (Figure 9C). Cardiovascular disease is a comorbidity that could result in higher levels of sAXL and sMERTK,³⁹ unrelated to NASH; however, no relationship with arterial hypertension was detected in our cohort of patients. In contrast, a clear tendency to increased sAXL levels was observed in patients with diabetes in all groups analyzed.

As AXL activation leads to proteolytic shedding of the AXL extracellular from the cell surface,²⁶ the increase in

sAXL levels may suggest hepatic accumulation of AXL during NAFLD progression. Accordingly, cirrhotic NASH patients exhibited hepatic AXL overexpression (Figure 9D), with main AXL staining in liver nonparenchymal cells. To better characterize AXL upregulation, we analyzed AXL (green) by immunofluorescence and compared it to α -SMA and F4/80 (red) hepatic distribution (Figure 9E). Most of the punctuated AXL signal overlapped (yellow) with α -SMA-positive cells ($48 \pm 21\%$) and with macrophages ($41 \pm 7\%$), in agreement with its predicted main expression in activated HSCs and KCs.

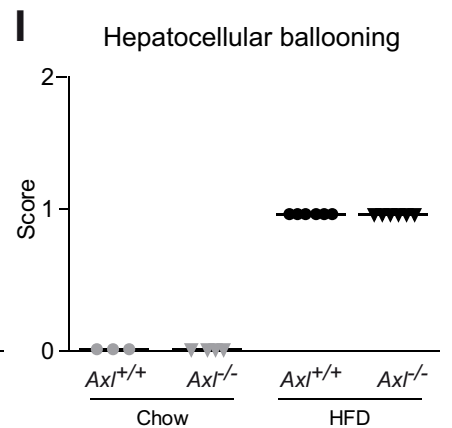
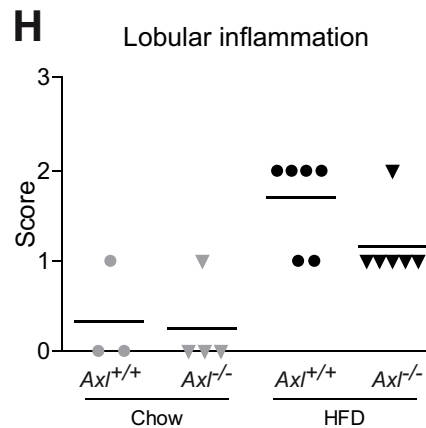
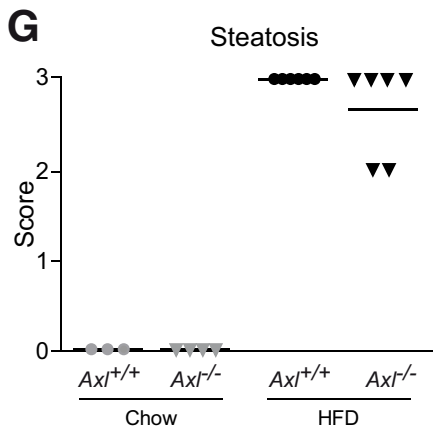
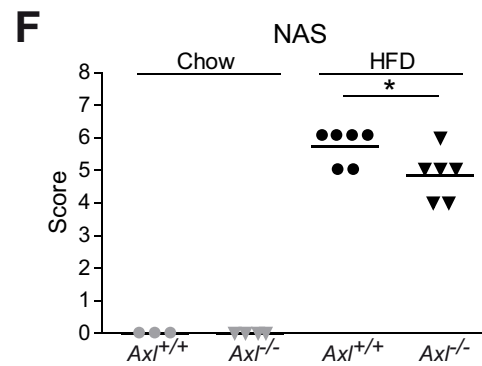
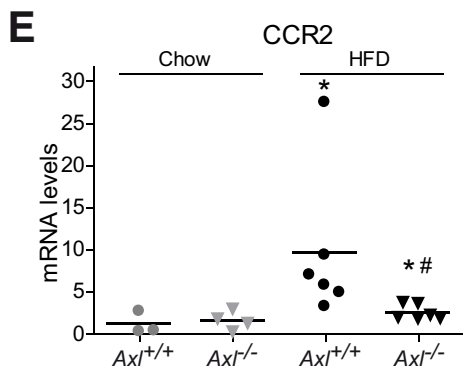
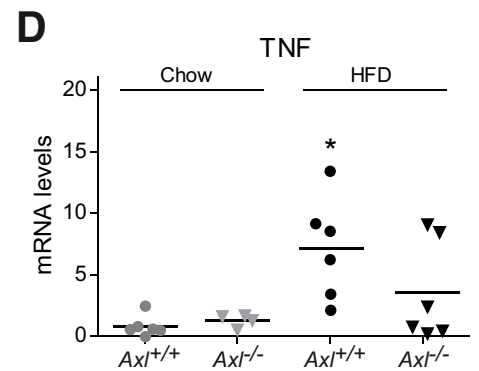
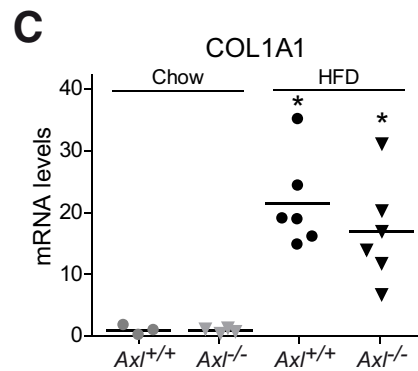
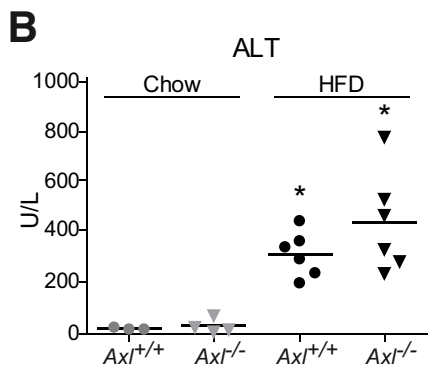
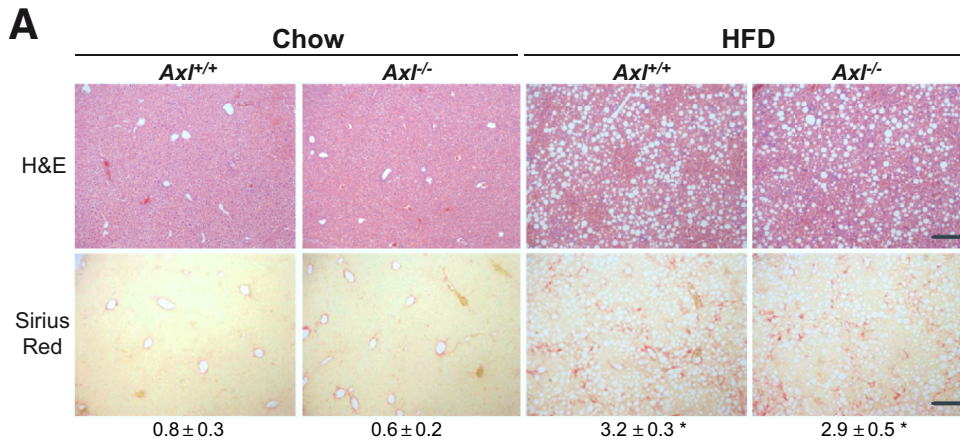
Bemcentinib Is Also Effective Reducing Liver Fibrosis and Inflammation in Early NASH

As our patients' data suggest that AXL activation is a mechanism upregulated already in initial stages of NAFLD, even before the onset of fibrosis, we decided to test if we could recapitulate the beneficial effects of AXL inhibition in an early NASH model. To do so, C57BL/6J mice were fed with a chow diet or HFD for 1 month, receiving bemcentinib or vehicle for the last 2 weeks. HFD-fed mice exhibited fatty liver, increased liver to body weight, elevated alanine aminotransferase transaminases and even the presence of some collagen deposition after 1 month (Figure 10A-C). Interestingly, bemcentinib reduced incipient fiber accumulation showing the importance of AXL signaling even in initial NAFLD stages. Similarly, the induction of profibrotic and inflammatory genes detected in HFD-fed liver was clearly reduced after AXL inhibition (Figure 10F, G). As *Axl*^{-/-} and *Mertk*^{-/-} mice share the same C57BL/6J background, AXL- and MERTK-deficient mice were included in the study. In agreement with previous results, *Mertk*^{-/-} mice displayed aggravated NASH pathology, with higher collagen deposition and liver inflammation. In contrast, *Axl*^{-/-} mice exhibited some protection after HFD feeding although not as important as after bemcentinib administration. Of note, HFD-fed *Axl*^{-/-} mice exhibited moderately increased GAS6 levels, but they were significantly less to the GAS6 increase detected in HFD-fed bemcentinib-treated mice (Figure 10D), suggesting GAS6-derived hepatoprotection as a contributing factor in bemcentinib efficacy.

Last, as sAXL was found increased in patients with simple steatosis with no detected fibrosis after liver biopsy, we wanted to verify this point in our animal model. After 2 weeks' HFD feeding, fat deposition but not collagen accumulation was observed in the livers of HFD-mice (Figure 10H). Interestingly, fibrosis and inflammation-related genes were already increased, as well as sAXL levels (Figure 10I), showing again a clear relationship between AXL activation and early NAFLD development.

Discussion

Several therapies are currently being evaluated to target NASH in a precirrhotic stage, when liver fibrosis and hepatic inflammation are still reversible. GAS6 and TAM receptors have been involved in other liver chronic pathologies; however, their therapeutic targeting in NASH has not been reported. According to our data, levels of soluble AXL are



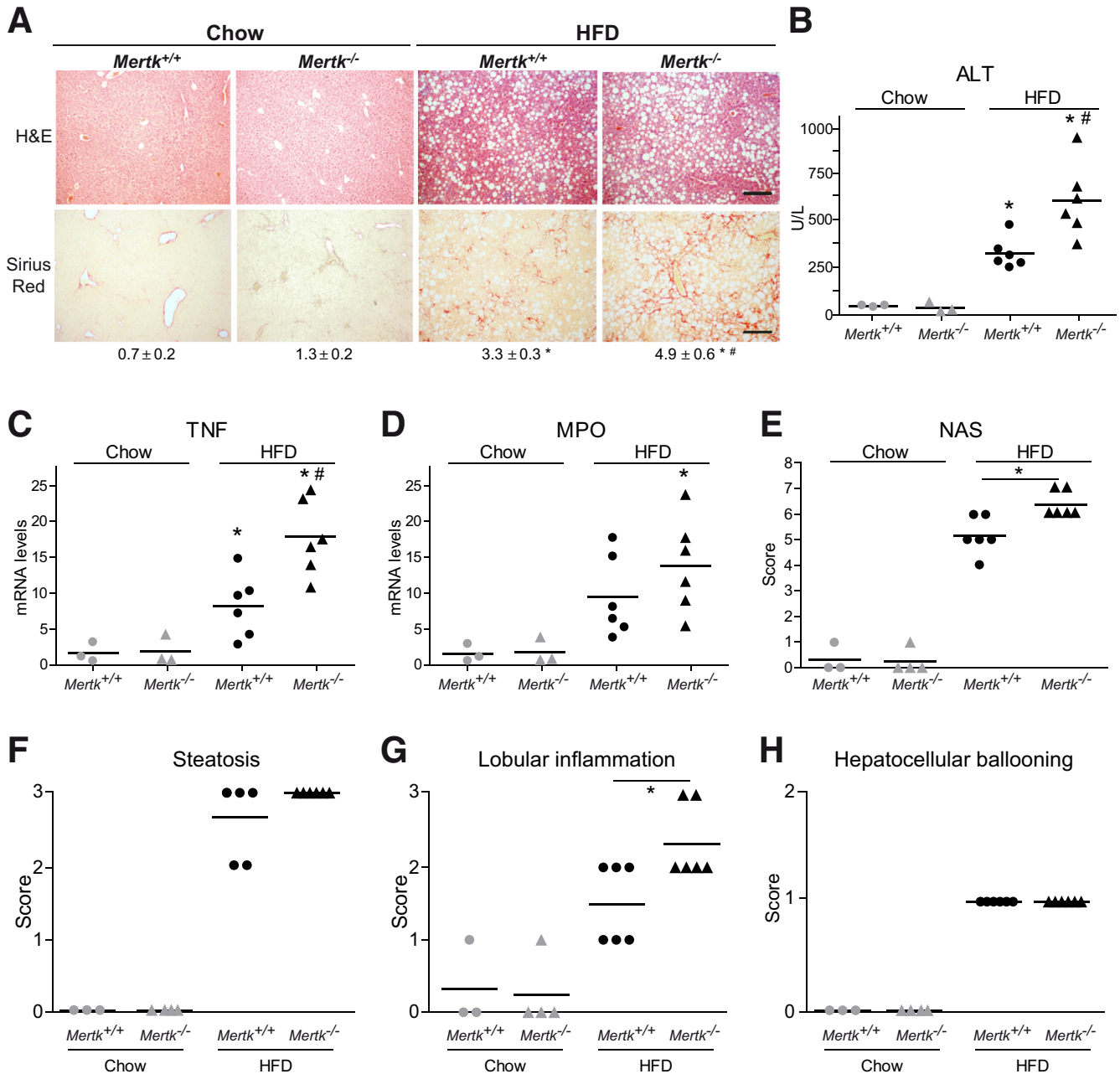


Figure 8. MERTK deficiency increased liver fibrosis and inflammation in HFD-fed mice. (A) Representative images of liver sections after H&E and Sirius Red staining from control and MERTK KO mice treated with chow or HFD diet. Scale bar = 200 μ m. Sirius Red quantification is shown below the respective pictures. Student's *t* test; * $P \leq .05$ vs control mice, # $P \leq .05$ vs HFD-fed mice; $n = 3-6$. (B) Alanine aminotransferase (ALT) serum levels from treated mice ($n = 3-6$). (C, D) mRNA expression level of TNF and MPO in liver samples from treated mice. * $P \leq .05$ vs control mice; # $P \leq .05$ vs HFD-fed mice; $n = 3-6$. (E) NAFLD activation score, composed by (F) steatosis, (G) lobular inflammation, and (H) hepatocellular ballooning, was evaluated in liver samples from treated mice. One-way analysis of variance. * $P \leq .05$ vs HFD-fed mice; $n = 3-6$. The results shown are representative for 2 independent experiments.

Figure 7. (See previous page). AXL-deficient mice display partial protection against liver fibrosis and inflammation in HFD-fed mice. (A) Representative images of liver sections after H&E and Sirius Red staining from control and AXL KO mice treated with chow or HFD diet. Scale bar = 200 μ m. Sirius Red quantification is shown below the respective pictures. Student's *t* test; * $P \leq .05$ vs control mice. (B) alanine aminotransferase (ALT) serum levels from treated mice ($n = 3-6$). (C-E) mRNA expression level of COL1A1, TNF, and CCR2 in liver samples from treated mice ($n = 3-6$). (F) NAFLD Activation Score, composed by (G) steatosis, (H) lobular inflammation, and (I) hepatocellular ballooning, was evaluated in liver samples from treated mice. One-way analysis of variance; * $P \leq .05$ vs HFD-fed mice; $n = 3-6$. The results shown are representative for 2 independent experiments.

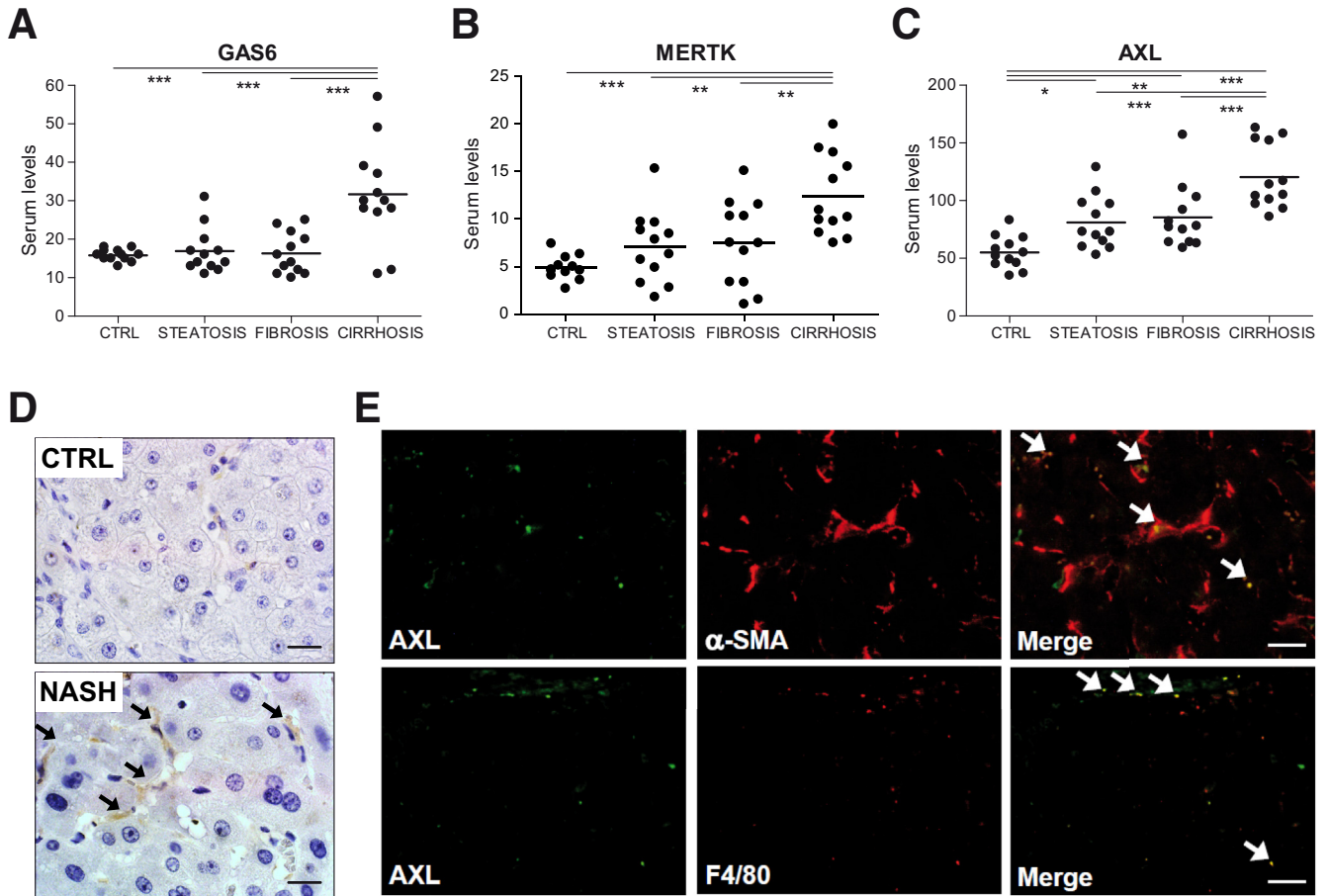


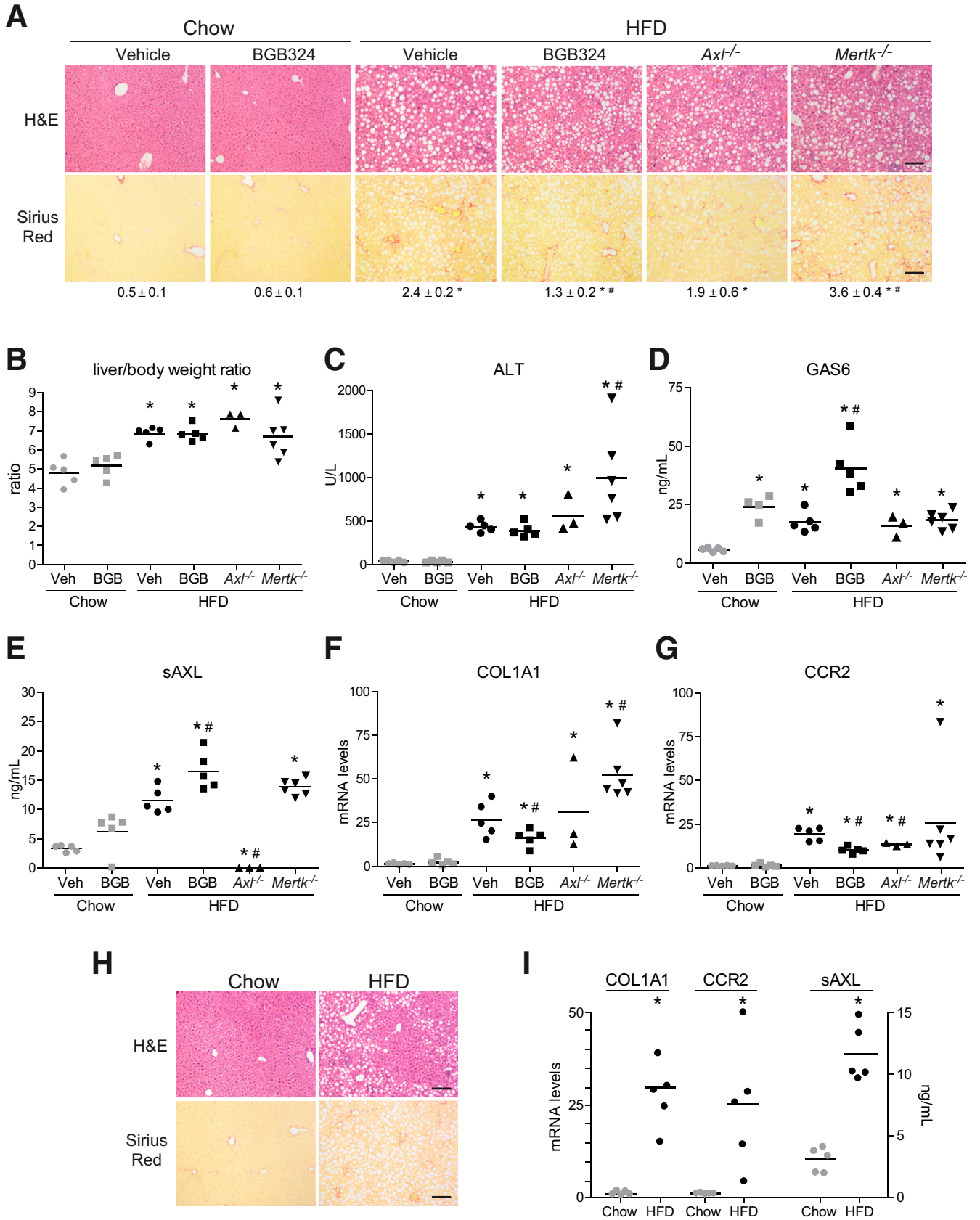
Figure 9. Serum levels of sAXL are increased in NASH patients being expressed in activated HSCs and KCs. (A–C) GAS6 and soluble levels of AXL and MERTK (ng/mL) were measured in control individuals ($n = 12$) and in patients with different degree of NASH progression: with steatosis ($n = 12$), fibrosis ($n = 12$), and cirrhosis ($n = 12$). $*P \leq .05$, $**P \leq .01$ and $***P \leq .001$ between groups (1-way analysis of variance). (D) Representative images of liver IHC of AXL expression in control and cirrhotic NASH patients. Scale bar = $50 \mu\text{m}$; $n = 4$. (E) Representative immunofluorescence images of AXL (green) and α -SMA/F480 (red) in cirrhotic NASH patients ($n = 4$).

increased in NAFLD patients reflecting that AXL signaling is activated in early NAFLD stages. Moreover, increased circulating sAXL, which is known to be bound to GAS6 in serum,⁴⁰ is probably capturing locally released GAS6 and reducing its cellular availability and its known hepatoprotective effect.¹⁷

We and others have shown previously the profibrotic capacities of GAS6 signaling, in the liver,^{21,22,37} and recently in other organs.⁴¹ Our present results reveal that GAS6 or AXL activation alone is enough to induce strong AKT phosphorylation and HSC activation, promoting profibrogenic extracellular changes and migration (Figure 6F), and reducing MCP-1 release and diminishing monocyte recruitment. In addition, AXL has a proinflammatory effect in primary KCs, which displayed reduced LPS-induced inflammatory gene expression in the presence of bemcentinib. Besides AXL inhibition, bemcentinib induces GAS6 upregulation, possibly as a compensatory mechanism. The hepatoprotective role of GAS6 via MERTK/AKT/STAT3, in line with previously observed GAS6-induced protection against hypoxia in primary hepatocytes,¹⁷ is evident in PMHs after palmitic acid exposure. The AKT/STAT3 role in hepatocellular lipotoxicity associated to NASH pathology has been

previously described.²⁷ However, the participation in this protection of GAS6/MERTK is novel information. In this sense, the GAS6 induction, observed in bemcentinib treated animals in comparison with $Axl^{-/-}$ mice, could be a distinctive mechanism that helps therapy based on small molecule inhibition to be more effective. Evidently, other direct and off targets effects may participate, similarly as we cannot discard a potential compensatory effect on AKL KO mice. For instance, recent data has shown that AXL inhibitors such as bemcentinib, by blocking AXL phosphorylation and subsequent ubiquitination,⁴² contribute to AXL and sAXL accumulation in cells and medium. However, bemcentinib good tolerability in patients, observed in trials, indicates that potential side effects are not of clinical importance.

Consistent with the in vitro data, bemcentinib showed a powerful antifibrotic response in NASH animal models. Interestingly, pharmacological inhibition of GAS6/AXL by bemcentinib showed better response in our animal NASH models than genetic ablation in $Axl^{-/-}$ mice. It is possible that bemcentinib targets the profibrotic and proinflammatory effect of AXL signaling, while preserving other liver protecting functions of the GAS6 system. In fact, $Axl^{-/-}$



mice did not exhibit changes in serum GAS6 levels, in contrast to the increase observed after bemcentinib administration. The protective role of GAS6 in ischemia/reperfusion-induced liver damage,¹⁷ and in liver wound healing response^{18,19} may support GAS6 as a hepatoprotective factor induced by bemcentinib. Moreover, the liver deterioration observed in *Mertk*^{-/-} mice corroborates the anti-inflammatory role of GAS6 in macrophages via MERTK. This result concurs with recent data underscoring the role of MERTK in the homeostatic resolution of inflammation after acute liver failure in human and experimental models, and the aggravated damage described in *Mertk*^{-/-} mice exposed to acetaminophen overdose.^{43,44} Therefore, despite the suggested anti-fibrotic effect of MERTK inhibitors in HSCs in vitro,²² dual AXL-MERTK inhibitors,^{45,46} with potential value in cancer treatment, may jeopardize the protection achieved by AXL blockade in NASH treatment. Regarding this point, bemcentinib has a very low inhibitory effect on MERTK, with an IC₅₀ 100 fold higher than for AXL, which is not reached in in vivo administration.²⁹ Certainly, achieving a receptor- and cell-specific inhibition of TAMs is a challenge to devise a useful strategy for NASH that could be translated to the clinic.

Interestingly, AXL inhibition by bemcentinib potentiates antitumor immune response,^{47,48} especially in combination with checkpoint inhibitors such as the anti-PD-1 agent nivolumab, recently Food and Drug Administration-approved for advanced liver cancer. In fact, other approved cancer drugs, such as cabozantinib and sunitinib, have potent activity against AXL, indicating that this inhibition may be well tolerated, or even beneficial, in the clinic.⁴⁹ In HCC patients, high levels of AXL and CXCL5 correlated with advanced tumor stages, recruitment of neutrophils into HCC tissue, and reduced survival.⁵⁰ Therefore, an antitumoral action of bemcentinib could be an additional benefit for NASH individuals, predisposed to develop liver cancer due to their protumorigenic liver microenvironment. The present use of bemcentinib in cancer patients for long time periods, with good safety and tolerability, underscores its potential for future clinical trials in NASH.

In summary, our results indicate that AXL is a receptor tyrosine kinase profibrogenic in HSCs and proinflammatory in KCs, while GAS6 protects the hepatocyte against lipotoxicity by MERTK signaling. AXL increase during NAFLD progression in patients and bemcentinib reduction of liver fibrosis and inflammation in experimental NASH supports AXL targeting as an interesting strategy in the treatment of human NASH.

Materials and Methods

Cell Culture and Treatments

Primary mouse hepatocytes, HSCs, and KCs were isolated as previously indicated.^{32,51,52} LX2 cells were kindly given by Dr Ramón Bataller.⁵³ Cells were treated with bemcentinib (0.25 μM; BerGenBio, Oslo, Norway), LPS (*Escherichia coli* 0111:B4, 50 ng/mL; Sigma-Aldrich, St. Louis, MO), ADAM10 inhibitor (GI254023X, 10 μM; Sigma-Aldrich), ADAM17 inhibitor (TMI005, 10 μM; Axon Medchem, Reston, VA), 1-μg/mL rGas6 (#986-GS, mouse; #885-GSB, human; R&D Systems, Minneapolis, MN), 10-nM AXL activating antibody (#AF854, mouse; #AF154, human 10 nM; R&D Systems), and MERTK activating antibody (#AF591, mouse; #AF891, human, 10 nM; R&D Systems) or normal Goat IgG Control (AB-108-C; R&D Systems). Cell death in primary mouse hepatocytes was evaluated by MTT assay and results were confirmed using standard trypan blue (0.2%) exclusion assays by optical microscopy.¹⁷

In Vivo Models

Animal studies, in accordance with the principles and procedures outlined in the National Institutes of Health Guide for the Care and Use of Laboratory Animals, were approved by the institutional animal care committee (Universitat de Barcelona). WT, *Axl*^{-/-} (Mouse Strain #005777; The Jackson Laboratory, Bar Harbor, ME) and *Mertk*^{-/-} (Dr Lemke Lab) male 8- to 10-week-old mice, all in the C57BL/6J background, were used. In experiments using *Axl*^{-/-} or *Mertk*^{-/-} mice, control sibling *Axl*^{+/+} or *Mertk*^{+/+} littermates were used. All mice were maintained with a 12-hour light/dark cycle (lights on at 8:00 AM) in a temperature-controlled environment. To induce NASH, mice were fed an MCD (Open Source diets #A02082002B) or an HFD (60% kcal) (Open Source diets #A06071302) diet for 6 or 8 weeks, respectively, receiving daily doses of bemcentinib (50 mg/kg twice daily) or vehicle by oral gavage for the last 2 weeks. Alanine and aspartate transaminases in serum samples and triglycerides and cholesterol levels from liver extracts were measured using a biochemical analyzer at the Clinic Hospital Core (Barcelona, Spain).

H&E, Sirius Red Staining, and NAS Index

Livers were formalin-fixed and 7-μm sections were routinely stained with H&E or a 0.1% Sirius Red-picric solution following standard procedures.^{21,51} The slices were examined with a Nikon (Tokyo, Japan) Eclipse E-1000 microscope equipped with an Olympus (Tokyo, Japan) DP72

Figure 10. (See previous page). Bemcentinib reduces early liver fibrosis and inflammation in HFD-fed mice. (A) Representative images of liver sections after H&E and Sirius Red staining from mice fed for 4 weeks with chow and HFD diet that received vehicle or bemcentinib (BGB324) gavages for the last 2 weeks. Scale bar = 200 μm. Sirius Red quantifications are shown under representative pictures. Student's *t* test; **P* ≤ .05 vs control mice; #*P* ≤ .05 vs HFD-fed mice; *n* = 3–6. (B) Liver to body weight and (C) serum alanine aminotransferase (ALT) transaminases were measured (n = 3–6). (D) Serum GAS6 and (E) sAXL were measured in mice fed with chow diet and HFD gavaged with vehicle or bemcentinib. One-way analysis of variance; **P* ≤ .05 vs chow-fed mice; #*P* ≤ .05 vs HFD-fed mice; *n* = 3–6. (F, G) mRNA expression level of COL1A1 and CCR2 in liver samples from treated mice. **P* ≤ .05 vs chow-fed mice; #*P* ≤ .05 vs HFD-fed mice; *n* = 3–6. (H) Representative images of liver sections after H&E and Sirius Red staining from mice fed for 2 weeks with chow and HFD diet. Scale bar = 200 μm. (I) mRNA expression level of COL1A1 and CCR2 in liver samples and protein sAXL levels in serum from treated mice. **P* ≤ .05 vs chow-fed mice; *n* = 5. The results shown are representative for 2 independent experiments.

camera. For collagen-fiber determination, a series of 6 random selected fields from each slice were visualized and quantified using ImageJ 1.48v software (National Institutes of Health, Bethesda, MD). NAFLD activity score (NAS) index was determined in H&E samples as previously reported.⁵⁴ In brief, NAS was assessed blindly evaluating the degree of steatosis (0–3), lobular inflammation (0–3), and ballooning (0–2). According to this algorithm, NAFLD requires the presence of steatosis in >5% of hepatocytes, and NASH, in addition to steatosis, of hepatocellular ballooning of any degree and focus of inflammatory cells within the lobule.

Immunohistochemical Staining

The 5- μ m liver sections (paraffin-embedded) were deparaffinized in xylene and dehydrated in graded alcohol series. Heat-induced antigen retrieval was performed in citrate buffer and endogenous peroxidase was blocked with 3% H₂O₂ solution. Slides were incubated with primary antibody (mouse anti- α -SMA: M0851, DAKO; rat anti-F4/80: sc-59171; Santa Cruz Biotechnology, Dallas, TX; rabbit anti-AXL: C89E7, Cell Signaling Technology, Danvers, MA) overnight in a wet chamber at 4°C. After rinsing with phosphate-buffered saline (PBS), the slides were incubated with a biotinylated antibody for 45 minutes in a wet chamber and developed with the ABC-HRP Kit (Vector Laboratories, Burlingame, CA) and peroxidase substrate DAB (Sigma-Aldrich). After rinsing the slides with tap water, they were counterstained with hematoxylin and mounted with Aquatex (Merck Millipore, Burlington, MA).

Immunofluorescence Staining

Paraffin molds containing liver sections were cut into 5- μ m sections. The sections were deparaffinized in xylene and dehydrated in graded alcohol series. Heat-induced antigen retrieval was performed in citrate buffer. Slides were incubated with primary antibody (mouse anti- α -SMA: M0851, DAKO; rat anti-F4/80: sc-59171; Santa Cruz Biotechnology; rabbit anti-AXL: C89E7; Cell Signaling) overnight in a wet chamber at 4°C. After rinsing with PBS, the slides were incubated with fluorescent secondary antibodies for 45 minutes in a wet chamber and mounted with ProLong Gold Antifade Mountant (Invitrogen, Carlsbad, CA).

Liver Collagen Determination

Levels of hepatic hydroxyproline, a specific component of collagen, were determined.^{21,51} Briefly, liver samples and 4-hydroxy-L-proline standards were hydrolyzed in 6N HCl at 120°C for 25 minutes. Free hydroxyproline from each hydrolysate was oxidized with Chloramine-T and after addition of Ehrlich reagent; absorbance was read at 550 nm. Data were normalized to liver wet weight.

MCP-1 and p-AKT Determination by ELISA

LX2 cells were seeded in 12-well plate (2×10^5 cells/well) in Dulbecco's modified Eagle medium/10% fetal bovine serum and allowed to attach and grow for >24 hours. Before experiments cells were left 6 hours in

Dulbecco's modified Eagle medium without fetal bovine serum, pretreated with bemcentinib for 60 minutes before addition of GAS6 (1 μ g/mL), for 16 hours for MCP-1 and for 15 minutes for p-AKT determination. Cell lysis was performed in 150 μ L/well of 1-mM EDTA, 0.5% Triton X-100, 5-mM NaF, 6-M urea, 1-mM activated sodium orthovanadate, 2.5-mM sodium pyrophosphate, 10- μ g/mL leupeptin, 10- μ g/mL pepstatin, 100- μ M PMSF, and 3- μ g/mL aprotinin in PBS, pH 7.2–7.4. For assay lysates were diluted 1:6 in 1-mM EDTA, 0.5% Triton X-100, and 5-mM NaF in PBS, pH 7.2–7.4. p-AKT standards were prepared in 1-mM EDTA, 0.5% Triton X-100, 5-mM NaF, 1-M urea in PBS, pH 7.2–7.4. The ELISA kit employed for p-AKT determination was DuoSet IC, Human/Mouse/Rat Phospho-Akt (Pan) (S473), Catalog Number DYC887-2 (R&D Systems). For MCP-1 secretion to extracellular media, the Human MCP-1 (CCL2) Mini TMB ELISA Development Kit (Cat#900-TM31; Peprotech, Rocky Hill, NJ) was used following manufacturer's instructions. Finally, color development was monitored using an ELISA plate reader at 450 nm with wavelength correction set at 620 nm.

Determination of GAS6, Soluble AXL (sAXL) and Soluble MERTK (sMERTK) Levels

sAXL and sMERTK levels were determined in human and mouse serum samples by specific sandwich ELISA using commercial kits (DuoSet ELISA; R&D Systems) and following manufacturer's instructions, and GAS6 was analyzed as described previously.⁵⁵

Cell Migration Assay

LX2 were plated in 6-well plates, and upon confluence, a scratch was made in cell layer with a 200- μ L sterile micropipette tip. Cells were treated with bemcentinib and AXL activating antibody. Cells were photographed at baseline ($t = 0$ hours) and after 24 hours using an Olympus IX-70 microscope. ImageJ software was used to measure scratch closure and percentage of closure relative to control was calculated.

Sodium Dodecyl Sulfate Protein Gel Electrophoresis and Immunoblot Analysis

Cell lysates were prepared in RIPA buffer (50-mM Tris-HCl, pH 8, 150-mM NaCl, 1% Nonidet P-40, 0.1% sodium dodecyl sulfate, 1% Triton X-100 plus proteinase inhibitors). Protein concentration was determined by Bradford assay, and samples containing 10–50 μ g were separated by sodium dodecyl sulfate protein gel electrophoresis. Proteins were transferred to nitrocellulose membranes. After this, membranes were blocked in 8% nonfat milk in 20-mM Tris-HCl, 150-mM NaCl, and 0.05% Tween 20 for 1 hour at room temperature. Anti-AKT (sc-8312; Santa Cruz Biotechnology) anti-phospho-AKT (#9271; Cell Signaling); phospho-AXL (#PA5-39729; Invitrogen), phospho-MERTK (#SAB4504621; Sigma-Aldrich), phospho-STAT3 (#9145S; Cell Signaling), anti-ADAM10 (#ab1997; Abcam, Cambridge, United Kingdom), anti-ADAM17

Table 1. Biochemical Data From Control Individuals and NASH Patients

	Steatosis (F0)	Fibrosis (F1–F3)	Cirrhosis (F4)	Control values
Men/women	9/3	10/2	8/4	7/5
Body mass index, kg/m ²	36.0 ± 2.2 ^a	32.6 ± 1.6 ^a	32.5 ± 1.4 ^a	<25
Age, y	57.0 ± 3.25	60.7 ± 2.0	63.5 ± 1.5	51.7 ± 10.4
Bilirubin, mg/dL	0.62 ± 0.06	0.74 ± 0.07	3.19 ± 1.50 ^a	0.2–1.0
Albumin, g/L	44.5 ± 0.6	44.1 ± 0.7	37.3 ± 1.8 ^{b,c}	35–50
Quick, %	94.9 ± 2.0	90.8 ± 2.6	73.2 ± 4.0 ^{b,c}	70–100
Creatinine, mg/dL	0.9 ± 0.1	0.9 ± 0.1	0.8 ± 0.1	0.6–1.2
AST, U/L	49.6 ± 13.1 ^a	40.6 ± 5.2 ^a	64.3 ± 9.2 ^{a,c}	10–40
ALT, U/L	80.0 ± 25.6 ^a	58.0 ± 9.4 ^a	55.2 ± 8.6 ^a	10–35
GGT, U/L	97.3 ± 36.6 ^a	131.4 ± 34.2 ^a	168.0 ± 37.1 ^a	5–40
Platelets (×10 ³ /mm ³)	218 ± 20	202 ± 15 ^b	130 ± 23 ^{b,c}	125–400
Leukocytes (×10 ³ /mm ³)	8.2 ± 0.9	6.7 ± 0.4	5.6 ± 0.8	3.5–11.0

Values are mean ± SEM. For the control group, serums from 12 individuals (7 men and 5 women with average age of 51.7 ± 10.4 years) with BMI <23 kg/m² were used to measure GAS6, sAXL, and sMERTK levels. Reference ranges for each biochemical parameter are provided, as established for normal individuals according to the Hospital Clínic Core Lab (Barcelona, Spain).

ALT, alanine aminotransferase; AST, aspartate aminotransferase; BMI, body mass index; GGT, γ -glutamyltransferase; NASH, nonalcoholic steatohepatitis.

^aOutside the range of control values.

^b $P \leq .05$ vs steatosis group (F0).

^c $P \leq .05$ vs fibrosis group (F1–F3).

(#sc-390859; Santa Cruz Biotechnology), anti-GAPDH (#ab181602; Abcam), and anti- β -actin-HRP (#A3854; Sigma-Aldrich).

RNA Isolation and Real-Time Polymerase Chain Reaction

Total RNA was isolated with TRIzol reagent; 1 μ g of RNA was reverse-transcribed with iScript cDNA Synthesis Kit (Bio-Rad Laboratories, Hercules, CA) and real-time polymerase chain reaction was performed with iTaq Universal SYBR Green Supermix (Bio-Rad Laboratories) following the manufacturer's instructions. The primers sequences used were:

mouse α -SMA, Fw 5'- ATG GCT CTG GGC TCT GTA AG -3' and Rv 5'- CCC ATT CCA ACC ATT ACT CC -3'

mouse Col1A1, Fw: 5'- GAG CGG AGA GTA CTG GAT CG -3' and Rv: 5'- GTT CGG GCT GAT GTA CCA GT -3'

mouse MMP9, Fw 5'- CAA ATT CTT CTG GCG TGT GA -3' and Rv 5'- CGG TTG AAG CAA AGA AGG AG -3'

mouse F4/80, Fw: 5'-TTT CCT CGC CTG CTT CTT C-3' and Rv: 5'-CCC CGT CTC TGT ATT CAA CC-3'

mouse CCR2, Fw: 5'-ATC CAC GGC ATA CTA TCA ACA TC-3' and Rv: 5'- CAA GGC TCA CCA TCA TCG TAG-3'

mouse MPO, Fw: 5'-TGC TGA AGA ACC TGG AGT TG-3' and Rv: 5'-AAA CCG ATC ACC ATC ACG TA-3'

mouse TNF, Fw: 5'- CTG AAC TTC GGG GTG ATC GGT-3' and Rv: 5'-ACG TGG GCT ACA GGC TTG TCA-3'

mouse MCP1, Fw: 5'-CAA GAA GGA ATG GGT CCA GA-3' and Rv: 5'-GCT GAA GAC CTT AGG GCA GA-3'

mouse ADAM10, Fw: 5'-AAG GGA TAT GCA ATG GCT TC-3' and Rv: 5'-TTG CCC ATT AAT GCA CAC TT-3'

mouse ADAM17, Fw: 5'- CTG GCA GAT AAC ATC GTT GG-3' and Rv: 5'- GAT GCG AAC AGA TGC TGA GT-3'

mouse β -actin, Fw: 5'-GAC GGC CAG GTC ATC ACT AT-3' and Rv: 5'-CGG ATG TCA ACG TCA CAC TT-3'

Gene Array

A predesigned 384-well mouse fibrosis panel for use with SYBR Green (Bio-Rad Laboratories) was used following the manufacturer's instructions. Briefly, after isolating RNA with the TRIzol reagent, the corresponding complementary DNA (cDNA) was synthesized using the iScript advanced cDNA synthesis kit (Bio-Rad Laboratories). Once cDNA is obtained the polymerase chain reaction mix is prepared (iQ Universal SYBR Green Supermix) and added to the 384-well plate in which all the primers are lyophilized. Results are corrected and normalized to the housekeeping genes β -actin and TBP.

Human Samples

We included a cohort of consecutive patients with NAFLD diagnosed by liver biopsy at the Hospital Clínic of Barcelona. Patients with alcoholic consumption were excluded to avoid misclassification. Patients were categorized in each group according to the presence of inflammation, steatosis and fibrosis in the liver biopsy. The

presence of steatohepatitis was described according to validated specific scoring system for NAFLD and fibrosis according to METAVIR score.⁵⁴ Our cohort encompasses the whole spectrum of NAFLD: patients with simple steatosis (n = 12), patients with steatohepatitis and fibrosis (F1–F3; n = 12), and patients with NAFLD cirrhosis (n = 12). As expected, patients presented features of metabolic syndrome, 64% (n = 23 of 36) had arterial hypertension, 36% (n = 13 of 36) had diabetes mellitus, 28% (n = 10 of 36) presented dyslipidemia, and 14% (n = 5 of 36) had concomitant cardiovascular disease. For the control group, serum from 12 individuals with BMI <25 kg/m² was used to measure GAS6, MERTK, and AXL levels. Additional biochemical data are shown (Table 1). Human liver slides from healthy individuals or cirrhotic NASH patients (without hepatocellular carcinoma) were from the Biobank of the Hospital Clínic. All subjects gave written informed consent in accordance with the Declaration of Helsinki, and the protocol, approved by ethical committees from the Hospital Clínic, followed ethical guidelines on handling human samples.

Statistical Analysis

All in vitro and in vivo experiments were repeated at least 3 times unless indicated. Statistical comparisons were performed using unpaired 2-tailed Student's *t* test or 1-way analysis of variance followed by Newman-Keuls multiple comparison test when indicated. All analyses were performed using GraphPad Prism 4 (GraphPad Software, San Diego, CA). A *P* value <.05 was considered significant.

All authors had access to the study data and reviewed and approved the final manuscript.

References

1. Younossi ZM, Loomba R, Rinella ME, Bugianesi E, Marchesini G, Neuschwander-Tetri BA, Serfaty L, Negro F, Caldwell SH, Ratziu V, Corey KE, Friedman SL, Abdelmalek MF, Harrison SA, Sanyal AJ, Lavine JE, Mathurin P, Charlton MR, Chalasani NP, Anstee QM, Kowdley KV, George J, Goodman ZD, Lindor K. Current and future therapeutic regimens for nonalcoholic fatty liver disease and nonalcoholic steatohepatitis. *Hepatology* 2018;68:361–371.
2. Rinella ME. Nonalcoholic fatty liver disease: a systematic review. *JAMA* 2015;313:2263–2273.
3. Younossi ZM, Koenig AB, Abdelatif D, Fazel Y, Henry L, Wymer M. Global epidemiology of nonalcoholic fatty liver disease—Meta-analytic assessment of prevalence, incidence, and outcomes. *Hepatology* 2016;64:73–84.
4. Schuppan D, Surabattula R, Wang XY. Determinants of fibrosis progression and regression in NASH. *J Hepatol* 2018;68:238–250.
5. Ratziu V, Harrison SA, Francque S, Bedossa P, Leheret P, Serfaty L, Romero-Gomez M, Boursier J, Abdelmalek M, Caldwell S, Drenth J, Anstee QM, Hum D, Hanf R, Roudot A, Megnier S, Staels B, Sanyal A, Group G-IS. Elafibranor, an agonist of the peroxisome proliferator-activated receptor- α and - δ , induces resolution of nonalcoholic steatohepatitis without fibrosis worsening. *Gastroenterology* 2016;150:1147–1159.e5.
6. Neuschwander-Tetri BA, Loomba R, Sanyal AJ, Lavine JE, Van Natta ML, Abdelmalek MF, Chalasani N, Dasarathy S, Diehl AM, Hameed B, Kowdley KV, McCullough A, Terrault N, Clark JM, Tonascia J, Brunt EM, Kleiner DE, Doo E, Network NCR. Farnesoid X nuclear receptor ligand obeticholic acid for non-cirrhotic, non-alcoholic steatohepatitis (FLINT): a multicentre, randomised, placebo-controlled trial. *Lancet* 2015;385:956–965.
7. Friedman SL, Ratziu V, Harrison SA, Abdelmalek MF, Aithal GP, Caballeria J, Francque S, Farrell G, Kowdley KV, Craxi A, Simon K, Fischer L, Melchor-Khan L, Vest J, Wiens BL, Vig P, Seyedkazemi S, Goodman Z, Wong VW, Loomba R, Tacke F, Sanyal A, Lefebvre E. A randomized, placebo-controlled trial of cenicriviroc for treatment of nonalcoholic steatohepatitis with fibrosis. *Hepatology* 2018;67:1754–1767.
8. Musso G, Cassader M, Gambino R. Non-alcoholic steatohepatitis: emerging molecular targets and therapeutic strategies. *Nat Rev Drug Discov* 2016;15:249–274.
9. Tsuchida T, Friedman SL. Mechanisms of hepatic stellate cell activation. *Nat Rev Gastroenterol Hepatol* 2017;14:397–411.
10. Hagstrom H, Nasr P, Ekstedt M, Hammar U, Stal P, Hultcrantz R, Kechagias S. Fibrosis stage but not NASH predicts mortality and time to development of severe liver disease in biopsy-proven NAFLD. *J Hepatol* 2017;67:1265–1273.
11. Hernandez-Gea V, Toffanin S, Friedman SL, Llovet JM. Role of the microenvironment in the pathogenesis and treatment of hepatocellular carcinoma. *Gastroenterology* 2013;144:512–527.
12. Couluouarn C, Clement B. Stellate cells and the development of liver cancer: therapeutic potential of targeting the stroma. *J Hepatol* 2014;60:1306–1309.
13. Barcena C, Stefanovic M, Tutusaus A, Martinez-Nieto GA, Martinez L, Garcia-Ruiz C, de Mingo A, Caballeria J, Fernandez-Checa JC, Mari M, Morales A. Angiogenin secretion from hepatoma cells activates hepatic stellate cells to amplify a self-sustained cycle promoting liver cancer. *Sci Rep* 2015;5:7916.
14. Lemke G, Rothlin CV. Immunobiology of the TAM receptors. *Nat Rev Immunol* 2008;8:327–336.
15. Graham DK, DeRyckere D, Davies KD, Earp HS. The TAM family: phosphatidylserine sensing receptor tyrosine kinases gone awry in cancer. *Nat Rev Cancer* 2014;14:769–785.
16. Fernandez-Fernandez L, Bellido-Martin L, Garcia de Frutos P. Growth arrest-specific gene 6 (GAS6). An outline of its role in haemostasis and inflammation. *Thromb Haemost* 2008;100:604–610.
17. Llacuna L, Barcena C, Bellido-Martin L, Fernandez L, Stefanovic M, Mari M, Garcia-Ruiz C, Fernandez-Checa JC, Garcia de Frutos P, Morales A. Growth arrest-specific protein 6 is hepatoprotective against murine ischemia/reperfusion injury. *Hepatology* 2010;52:1371–1379.

18. Couchie D, Lafdil F, Martin-Garcia N, Laperche Y, Zafrani ES, Mavier P. Expression and role of Gas6 protein and of its receptor Axl in hepatic regeneration from oval cells in the rat. *Gastroenterology* 2005; 129:1633–1642.
19. Lafdil F, Chobert MN, Deveaux V, Zafrani ES, Mavier P, Nakano T, Laperche Y, Brouillet A. Growth arrest-specific protein 6 deficiency impairs liver tissue repair after acute toxic hepatitis in mice. *J Hepatol* 2009;51:55–66.
20. Lafdil F, Chobert MN, Couchie D, Brouillet A, Zafrani ES, Mavier P, Laperche Y. Induction of Gas6 protein in CCl₄-induced rat liver injury and anti-apoptotic effect on hepatic stellate cells. *Hepatology* 2006;44:228–239.
21. Barcena C, Stefanovic M, Tutusaus A, Joannas L, Menendez A, Garcia-Ruiz C, Sancho-Bru P, Mari M, Caballeria J, Rothlin CV, Fernandez-Checa JC, de Frutos PG, Morales A. Gas6/Axl pathway is activated in chronic liver disease and its targeting reduces fibrosis via hepatic stellate cell inactivation. *J Hepatol* 2015; 63:670–678.
22. Petta S, Valenti L, Marra F, Grimaudo S, Tripodo C, Bugianesi E, Camma C, Cappon A, Di Marco V, Di Maira G, Dongiovanni P, Rametta R, Gulino A, Mozzi E, Orlando E, Maggioni M, Pipitone RM, Fargion S, Craxi A. MERTK rs4374383 polymorphism affects the severity of fibrosis in non-alcoholic fatty liver disease. *J Hepatol* 2016;64:682–690.
23. Musso G, Cassader M, De Michieli F, Paschetta E, Pinach S, Saba F, Bongiovanni D, Framarin L, Berrutti M, Leone N, Corvisieri S, Parente R, Molinaro F, Sircana A, Bo S, Gambino R. MERTK rs4374383 variant predicts incident nonalcoholic fatty liver disease and diabetes: role of mononuclear cell activation and adipokine response to dietary fat. *Hum Mol Genet* 2017;26:1747–1758.
24. Mari M, Tutusaus A, Garcia de Frutos P, Morales A. Genetic and clinical data reinforce the role of GAS6 and TAM receptors in liver fibrosis. *J Hepatol* 2016; 64:983–984.
25. Sheridan C. First Axl inhibitor enters clinical trials. *Nat Biotechnol* 2013;31:775–776.
26. Zagorska A, Traves PG, Lew ED, Dransfield I, Lemke G. Diversification of TAM receptor tyrosine kinase function. *Nat Immunol* 2014;15:920–928.
27. Guo R, Nair S, Zhang Y, Ren J. Adiponectin deficiency rescues high-fat diet-induced hepatic injury, apoptosis and autophagy loss despite persistent steatosis. *Int J Obes (Lond)* 2017;41:1403–1412.
28. Han J, Bae J, Choi CY, Choi SP, Kang HS, Jo EK, Park J, Lee YS, Moon HS, Park CG, Lee MS, Chun T. Autophagy induced by AXL receptor tyrosine kinase alleviates acute liver injury via inhibition of NLRP3 inflammasome activation in mice. *Autophagy* 2016; 12:2326–2343.
29. Holland SJ, Pan A, Franci C, Hu Y, Chang B, Li W, Duan M, Torneros A, Yu J, Heckrodt TJ, Zhang J, Ding P, Apatira A, Chua J, Brandt R, Pine P, Goff D, Singh R, Payan DG, Hitoshi Y. R428, a selective small molecule inhibitor of Axl kinase, blocks tumor spread and prolongs survival in models of metastatic breast cancer. *Cancer Res* 2010;70:1544–1554.
30. Richard AS, Shim BS, Kwon YC, Zhang R, Otsuka Y, Schmitt K, Berri F, Diamond MS, Choe H. AXL-dependent infection of human fetal endothelial cells distinguishes Zika virus from other pathogenic flaviviruses. *Proc Natl Acad Sci U S A* 2017;114:2024–2029.
31. Caballero F, Fernandez A, Matias N, Martinez L, Fucho R, Elena M, Caballeria J, Morales A, Fernandez-Checa JC, Garcia-Ruiz C. Specific contribution of methionine and choline in nutritional nonalcoholic steatohepatitis: impact on mitochondrial S-adenosyl-L-methionine and glutathione. *J Biol Chem* 2010; 285:18528–18536.
32. de Mingo A, de Gregorio E, Moles A, Tarrats N, Tutusaus A, Colell A, Fernandez-Checa JC, Morales A, Mari M. Cysteine cathepsins control hepatic NF-kappaB-dependent inflammation via sirtuin-1 regulation. *Cell Death Dis* 2016;7:e2464.
33. Matsumoto M, Hada N, Sakamaki Y, Uno A, Shiga T, Tanaka C, Ito T, Katsume A, Sudoh M. An improved mouse model that rapidly develops fibrosis in non-alcoholic steatohepatitis. *Int J Exp Pathol* 2013; 94:93–103.
34. Orme JJ, Du Y, Vanarsa K, Mayeux J, Li L, Mutwally A, Arriens C, Min S, Hutcheson J, Davis LS, Chong BF, Satterthwaite AB, Wu T, Mohan C. Heightened cleavage of Axl receptor tyrosine kinase by ADAM metalloproteases may contribute to disease pathogenesis in SLE. *Clin Immunol* 2016;169:58–68.
35. Atapattu L, Saha N, Chheang C, Eissman MF, Xu K, Vail ME, Hii L, Llerena C, Liu Z, Horvay K, Abud HE, Kusebauch U, Moritz RL, Ding BS, Cao Z, Rafii S, Ernst M, Scott AM, Nikolov DB, Lackmann M, Janes PW. An activated form of ADAM10 is tumor selective and regulates cancer stem-like cells and tumor growth. *J Exp Med* 2016;213:1741–1757.
36. Fiorentino L, Vivanti A, Cavalera M, Marzano V, Ronci M, Fabrizi M, Menini S, Pugliese G, Menghini R, Khokha R, Lauro R, Urbani A, Federici M. Increased tumor necrosis factor alpha-converting enzyme activity induces insulin resistance and hepatosteatosis in mice. *Hepatology* 2010;51:103–110.
37. Stauffer K, Dengler M, Huber H, Marculescu R, Stauber R, Lackner C, Dienes HP, Kivaranovic D, Schachner C, Zeitlinger M, Wulkersdorfer B, Rauch P, Prager G, Trauner M, Mikulits W. The non-invasive serum biomarker soluble Axl accurately detects advanced liver fibrosis and cirrhosis. *Cell Death Dis* 2017;8:e3135.
38. Dengler M, Stauffer K, Huber H, Stauber R, Bantel H, Weiss KH, Starlinger P, Pock H, Kloters-Plachky P, Gotthardt DN, Rauch P, Lackner C, Stift J, Brostjan C, Gruenberger T, Kumada T, Toyoda H, Tada T, Weiss TS, Trauner M, Mikulits W. Soluble Axl is an accurate biomarker of cirrhosis and hepatocellular carcinoma development: results from a large scale multicenter analysis. *Oncotarget* 2017;8:46234–46248.
39. McShane L, Tabas I, Lemke G, Kurowska-Stolarska M, Maffia P. TAM receptors in cardiovascular disease. *Cardiovasc Res* 2019;115:1286–1295.
40. Ekman C, Gottsater A, Lindblad B, Dahlback B. Plasma concentrations of Gas6 and soluble Axl correlate with

- disease and predict mortality in patients with critical limb ischemia. *Clin Biochem* 2010;43:873–876.
41. Espindola MS, Habel DM, Narayanan R, Jones I, Coelho AL, Murray LA, Jiang D, Noble PW, Hogaboam CM. Targeting of TAM receptors ameliorates fibrotic mechanisms in idiopathic pulmonary fibrosis. *Am J Respir Crit Care Med* 2018;197:1443–1456.
 42. Lauter M, Weber A, Torka R. Targeting of the AXL receptor tyrosine kinase by small molecule inhibitor leads to AXL cell surface accumulation by impairing the ubiquitin-dependent receptor degradation. *Cell Commun Signal* 2019;17:59.
 43. Triantafyllou E, Pop OT, Possamai LA, Wilhelm A, Liaskou E, Singanayagam A, Bernsmeier C, Khamri W, Petts G, Dargue R, Davies SP, Tickle J, Yuksel M, Patel VC, Abeles RD, Stamataki Z, Curbishley SM, Ma Y, Wilson ID, Coen M, Woollard KJ, Quaglia A, Wendon J, Thursz MR, Adams DH, Weston CJ, Antoniadou CG. MerTK expressing hepatic macrophages promote the resolution of inflammation in acute liver failure. *Gut* 2018; 67:333–347.
 44. Mukherjee SK, Wilhelm A, Antoniadou CG. TAM receptor tyrosine kinase function and the immunopathology of liver disease. *Am J Physiol Gastrointest Liver Physiol* 2016;310:G899–G905.
 45. Kim JE, Kim Y, Li G, Kim ST, Kim K, Park SH, Park JO, Park YS, Lim HY, Lee H, Sohn TS, Kim KM, Kang WK, Lee J. MerTK inhibition by RXDX-106 in MerTK activated gastric cancer cell lines. *Oncotarget* 2017; 8:105727–105734.
 46. Gilmour MSA, Ottmann OG, Hills RK, Knapper S, Zabkiewicz J. AXL/ Mer inhibitor ONO-9330547 as a novel therapeutic agent in a stromal co-culture model of primary acute myeloid leukaemia (AML). *Blood* 2016; 128:2754.
 47. Guo Z, Li Y, Zhang D, Ma J. Axl inhibition induces the antitumor immune response which can be further potentiated by PD-1 blockade in the mouse cancer models. *Oncotarget* 2017;8:89761–89774.
 48. Ludwig KF, Du W, Sorrelle NB, Wnuk-Lipinska K, Topalovski M, Toombs JE, Cruz VH, Yabuuchi S, Rajeshkumar NV, Maitra A, Lorens JB, Brekken RA. Small-molecule inhibition of Axl targets tumor immune suppression and enhances chemotherapy in pancreatic cancer. *Cancer Res* 2018;78:246–255.
 49. Ferguson FM, Gray NS. Kinase inhibitors: the road ahead. *Nat Rev Drug Discov* 2018;17:353–377.
 50. Haider C, Hnat J, Wagner R, Huber H, Timelthaler G, Grubinger M, Coulouarn C, Schreiner W, Schlangen K, Sieghart W, Peck-Radosavljevic M, Mikulits W. Transforming growth factor-beta and Axl induce CXCL5 and neutrophil recruitment in hepatocellular carcinoma. *Hepatology* 2019;69:222–236.
 51. Moles A, Tarrats N, Fernandez-Checa JC, Mari M. Cathepsins B and D drive hepatic stellate cell proliferation and promote their fibrogenic potential. *Hepatology* 2009; 49:1297–1307.
 52. Mari M, Caballero F, Colell A, Morales A, Caballeria J, Fernandez A, Enrich C, Fernandez-Checa JC, Garcia-Ruiz C. Mitochondrial free cholesterol loading sensitizes to TNF- and Fas-mediated steatohepatitis. *Cell Metab* 2006;4:185–198.
 53. Xu L, Hui AY, Albanis E, Arthur MJ, O'Byrne SM, Blaner WS, Mukherjee P, Friedman SL, Eng FJ. Human hepatic stellate cell lines, LX-1 and LX-2: new tools for analysis of hepatic fibrosis. *Gut* 2005;54:142–151.
 54. Bedossa P, Poitou C, Veyrie N, Bouillot JL, Basdevant A, Paradis V, Tordjman J, Clement K. Histopathological algorithm and scoring system for evaluation of liver lesions in morbidly obese patients. *Hepatology* 2012; 56:1751–1759.
 55. Recarte-Pelz P, Tassies D, Espinosa G, Hurtado B, Sala N, Cervera R, Reverter JC, de Frutos PG. Vitamin K-dependent proteins GAS6 and Protein S and TAM receptors in patients of systemic lupus erythematosus: correlation with common genetic variants and disease activity. *Arthritis Res Ther* 2013;15:R41.

Received April 26, 2019. Accepted October 28, 2019.

Correspondence

Address correspondence to: Montserrat Marí, PhD, Albert Morales, PhD, or Pablo García de Frutos, PhD, Instituto de Investigaciones Biomédicas de Barcelona (IIBB-CSIC), C/ Rosselló 161, 6th Floor, 08036 Barcelona, Spain. e-mail: monmari@clinic.cat, amorales@clinic.cat, or pablo.garcia@iibb.csic.es; fax: +34-93-3638301.

Acknowledgments

The authors thank Dr Greg Lemke for providing *Mertk*^{-/-} mice and his critical reading of the manuscript, and Dr Alan Holmes for his insightful comments.

Conflicts of interest

These authors disclose the following: James B. Lorens is a co-founder of BerGenBio. Gro Gausdal is employed by BerGenBio. Pablo García de Frutos, Montserrat Marí, and Albert Morales received research funding from BerGenBio. The remaining authors disclose no conflicts.

Funding

This study was funded by grants from Instituto de Salud Carlos III (PI16/00930 and PI19/01410 to Montserrat Marí) and CIBEREHD; Ministerio de Economía y Competitividad (SAF2015-66515-R and RTI2018-095672-B-I00 to Albert Morales and Pablo García de Frutos, and RTI2018-095572-B-I00 to Anna Colell), and co-funded by FEDER (Fondo Europeo de Desarrollo Regional, Unión Europea), Fundació Marató de TV3 (to Pablo García de Frutos), AGAUR (2017_SGR_177 to Albert Morales), and CERCA Programme/ Generalitat de Catalunya.